Cement and Concrete Research 147 (2021) 106514

Contents lists available at ScienceDirect

Cement and Concrete Research

journal homepage: www.elsevier.com/locate/cemconres

Impact of downhole pressure and fluid-access on the effectiveness of wellbore cement expansion additives

T.K.T. Wolterbeek [a,*], E.K. Cornelissen [b], S.J.T. Hangx [a], C.J. Spiers [a]

[a] Department of Earth Sciences, Utrecht University, Princetonlaan 4, 3584 CB Utrecht, the Netherlands
[b] Shell Global Solutions International B.V., Grasweg 31, 1031 HW Amsterdam, the Netherlands

ARTICLE INFO

Keywords:
Oil well cement
Shrinkage
Expansion
MgO
Hydration
Annular fluid migration
Sustained casing pressure

ABSTRACT

Autogenous shrinkage of wellbore cement widely impairs zonal isolation. MgO-based cement expansion additives (CEAs) can mitigate this shrinkage, or even impart net expansion, by creating porosity through displacive crystal growth-processes. However, both MgO hydration and autogenous shrinkage behaviour depend strongly on stress state. Evaluation of CEA performance in wellbore cements therefore requires testing under elevated pressures representative for subsurface environments. We report experiments addressing the chemical and bulk volume changes that occur in cement hydrating at 10 MPa confining pressure and 90 °C. Volumetric response was investigated as function of MgO concentration, external water supply, and pore pressure decrease through water consumption during reaction. Results show the bulk expansion achieved using MgO-based CEAs diminishes markedly with increasing effective confining pressure or, equivalently, upon restricting fluid supply. This reduced expansion-potential under pressure has profound implications for slurry design, notably regarding CEA-concentrations required to counteract micro-annulus formation while maintaining low cement permeability.

1. Introduction

Portland cements have been applied in wellbores since the nineteenth century [1] and nowadays their use is essentially standard practice [2]. During wellbore drilling and construction, cement is placed in annular spaces between the casings and rock formations exposed to the borehole. Cement is also widely used for well plugging-and-abandonment (P&A). In both cases, the main purpose of cementing is to achieve zonal isolation, i.e., provide barriers against fluid seepage along the well trajectory. This is not so easily accomplished, however, as evidenced by widespread occurrence of sustained casing pressure and surface casing vent flow issues [3–5].

From a cementing viewpoint, seepage can have various causes. Cracks in the cement or micro-annuli along interfaces with the casings and rock undermine the sealing integrity provided by the low matrix permeability of Portland cement [6,7]. These defects may develop gradually, e.g. due to variations in temperature [8,9] or stress state experienced during field operations [10–15], but can also originate upon well construction or P&A [16,17]. Contamination of the cement may lead to dramatic changes in setting-time or final properties [18–21]. Incomplete coverage can result in mud channels, particularly along inclined wells [22–24]. Effective placement techniques will therefore always be essential.

Even under ideal placement conditions, however, Portland cements tend to exhibit so-called autogenous shrinkage [25–29]. Caused by the negative volume change of reaction associated with cement hydration [30–35], autogenous shrinkage occurs upon setting and produces a bulk volumetric contraction, which may result in tensile failure [26,36] or micro-annulus formation along casing-cement-rock interfaces [37–40]. Autogenous shrinkage is widely regarded as a key contributor to loss of zonal isolation [17,38,41–44]. Significant effort has been directed at understanding and measuring the volume evolution of wellbore cements [25,37,40,45–55]. These works showed that the amount of autogenous shrinkage depends strongly on experimental conditions during cement hydration, including the i) degree of access to external water sources and ii) confining pressure imposed [37,45,48].

Several strategies have been developed to mitigate autogenous shrinkage. Surfactants known as shrinkage reducing admixtures (SRAs) decrease the development of capillary forces during self-desiccation [56–58], which contribute to autogenous and drying shrinkage under atmospheric conditions [29,36,59–61]. So-called “internal curing” methods rely on the addition of superabsorbent or micro-porous

* Corresponding author.
E-mail address: T.K.T.Wolterbeek@uu.nl (T.K.T. Wolterbeek).

https://doi.org/10.1016/j.cemconres.2021.106514
Received 24 November 2020; Received in revised form 13 April 2021; Accepted 3 June 2021
Available online 15 June 2021

materials that act as tiny reservoirs inside the cement, which reduce autogenous shrinkage effects by supplying water to the ongoing hydration reactions [62–66]. Various fibres [67–69] and fillers [70] have also been applied.

The above approaches aim to inhibit the capillary tension, sorption-desorption and creep mechanisms underlying autogenous shrinkage [28,29]. Strategies involving so-called cement expansion additives (CEAs) instead aim to compensate for these compactive processes, by introducing expansive mechanisms that counteract their impact, thereby limiting bulk shrinkage or even imparting net expansive properties [53]. Two principal categories of CEAs can be distinguished, where expansion is accomplished via either i) displacive crystal growth, or ii) internal gas generation. Gas-generating CEAs include zinc or aluminium powders [71] and nitrogen-evolving additives [72]. Gas-generating systems are strongly affected by temperature and pressure, requiring careful slurry design and stabilisation to prevent gas bubbles from coalescing and potentially creating channels [2,41], while their overall effectiveness is limited to relatively low pressures.

Displacive crystal growth-based CEAs have been considered and applied in wellbore cementing for several decades, with varying degrees of success. They employ force of crystallisation (FoC)-producing reactions, where the growing crystals are capable of exerting mechanical force on their surroundings [73–87]. FoC-producing systems known to create expansion in cement include: i) precipitation of hydrated salts such as sodium sulphate [2,71,88–90], ii) delayed ettringite formation [2,90–95] and iii) the hydration of CaO and MgO [40,41,45,90,96–104]. Here discussions will focus on MgO, but many of the principles also apply to the other FoC-based CEAs.

How effectively displacive crystal growth can cause expansion in hydrating cement depends on various factors. Firstly, FoC-producing reactions must be thermodynamically viable under the chemical, pressure and temperature conditions of interest. Ettringite, for example, becomes unstable above 50 °C in Portland cements with Al_2O_3/SO_3 ratios >1.3 [105]. Naturally, this limits the application range of sulphoaluminate-based CEAs, which rely on ettringite formation. Ettringite may persist to higher temperatures, but its expansion-potential decreases rapidly towards 75 °C [106]. Secondly, displacive crystal growth must take place at the right moment. If crystallisation occurs while the cement still behaves slurry-like, there is no load-bearing solid framework that can sustain the forces needed for bulk volume expansion. Very slow crystallisation may also be undesirable, both from a practical perspective and because continued FoC-development after the cement has fully set might under certain conditions induce damage [40]. Ideally, the reactivity of CEAs should therefore be designed such that displacive crystal growth occurs largely when the hydrating cement has formed a solid framework capable of transferring the imposed displacements, but has not yet fully hardened [41].

The reactivity of MgO and CaO-based CEAs can to some extent be influenced during manufacturing, by tailoring the calcination temperature or heat treatment after synthesis. This produces “light burnt” (700–1000 °C), “hard burnt” (1000–1500 °C) and “dead burnt” (>1500 °C) versions, where reactivity decreases with increasing temperature. Even dead burnt CaO remains highly reactive [40,107], restricting its use to mitigation of early age shrinkage and low temperature applications. For MgO, three categories have been defined based on the particles' specific surface area, agglomeration, and hydration characteristics: “highly reactive”, “medium reactive” and “less reactive” [41,108], corresponding roughly to the above temperature windows. Increasing control on the properties of MgO allows CEAs to be optimised for the temperature and cement chemistry of interest [41,42,103,109,110].

The impact of downhole setting conditions on the effectiveness of CEA-modified “expanding cements” has received comparatively little attention [45,53], especially considering that confining pressure and external fluid-access are known to have profound effects on autogenous shrinkage in conventional, non-expanding cements [37,45,48]. In unrestrained settings, like buildings or roads, excessive expansion due to displacive crystal growth may lead to cracking and mechanical integrity loss, a condition called “unsoundness” [41,111–113]. Cement manufacturers therefore even avoid impurities that cause such effects, like free lime [2,114,115]. For similar reasons, the expanding cements used in civil engineering applications generally contain relatively low concentrations of MgO-based CEAs (typically <5% [103]). However, both the stress-strain-reaction behaviour of displacive crystal growth processes [76,77,86] and the mechanical behaviour of Portland cements [13,35,116–119] depend strongly on the degree of confinement. In downhole wellbore environments, cement hydrates under elevated (lithostatic) pressures and is generally restrained by the casing and surrounding rock formations [2], which may inhibit expansion and thereby significantly change cement volumetric behaviour at 1–4 km depth.

To confidently assess CEA-performance in expanding wellbore cements, the volumetric evolution during hydration and setting must be evaluated under conditions representative for downhole environments. This study presents a series of so-called LABCAT experiments [38], which enable measurement of the chemical shrinkage and changes in external dimensions (i.e. autogenous shrinkage or bulk volume change) that occur in cement samples hydrating under confining pressure and restricted water-access conditions. The volumetric evolution of a series of MgO-based expanding cements (at 90 °C and 10 MPa confining pressure) was systematically studied as a function of i) CEA concentration, ii) degree of external water-access and iii) maximum effective confining pressure allowed to develop during hydration due to self-desiccation. The results show that the bulk expansion-effect achievable using MgO-based CEAs diminishes markedly with increasing effective confining stress, which has profound implications for cement slurry design for subsurface applications.

2. Background and volume change terminology

The hydration and setting of Portland cement involve chemical reactions where the compound volume of the products, e.g. portlandite and calcium silicate hydrate (C-S-H) phases, is lower than the initial volume of the reactants, i.e. cement clinker phases plus water [30–34]. This “chemical shrinkage”, ΔV_{chem} [m^3], is related to the thermodynamic volume changes of reaction, $\Delta_r V^{PT}$ [m^3 mol^{-1}], associated with the x different hydration reactions operating in the cement:

$$\Delta V_{chem} = \sum \Delta_r V_x^{PT} d\xi_x \quad (1)$$

where ξ_x [mol] denotes extent of reaction. The complex chemistry (e.g. variable C-S-H properties) generally prevents useful application of Eq. (1) to real cements, but the expected $\Delta_r V^{PT}$ for individual, idealised reactions can be calculated (Table 1). Note the cement reactions involve a relative increase in solid volume (see $\Delta_r V_s^{PT}/V_{s,\,0}$ [%]), but show net shrinkage when the combined volume of solids and fluids is considered (see $\Delta_r V^{PT}/V_0$ [%]). Qualitatively, this can be explained by rearrangement of the water molecules, which adopt a more structured, higher density configuration upon incorporation into the solid [33,90].

The volume changes in Table 1 are defined at constant pressure and temperature. In reality, the chemical shrinkage must either be compensated for by other processes occurring inside the volume of cement, or be accommodated by a change in the external dimensions of the system:

$$\Delta V_{chem} + \Delta V_{int} = \Delta V_{ext} \quad (2)$$

Here, $\Delta V_{chem} < 0$ for cement hydration and ΔV_{int} [m^3] denotes the combined volumetric impact of possible i) changes in internal (pore) fluid pressure, ii) changes in the stress state of the solid matrix, iii) pore volume changes and associated cavitation or pore vapor phase formation, and iv) influx of matter, e.g. externally sourced water [25,28,120]. Note the first three factors represent effects caused by deviation from

Table 1
Molar volume change of reaction data (25 °C, 1 bar) for selected cement and metal oxide hydration reactions.

Reaction	$\Delta_r V^{PT}$ [cm^3 mol^{-1}]	$\Delta_r V_s^{PT}$ [cm^3 mol^{-1}]	$\Delta_r V^{PT}/V_0$ [%]	$\Delta_r V_s^{PT}/V_{s,0}$ [%]
$C_3S + 3.43\ H \longrightarrow C_{1.67}SH_{2.1} + 1.33\ CH$	−12.85	48.89	−9.54	66.97
$C_3S + 3.47\ H \longrightarrow C_{0.83}SH_{1.3} + 2.17\ CH$	−4.85	57.61	−3.58	78.92
$C_2S + 2.43\ H \longrightarrow C_{1.67}SH_{2.1} + 0.33\ CH$	−6.85	36.89	−7.15	70.94
$C_2S + 2.47\ H \longrightarrow C_{0.83}SH_{1.3} + 1.17\ CH$	1.15	45.61	1.19	87.71
$MgO + H_2O \longrightarrow Mg(OH)_2$	−4.50	13.50	−15.25	117.39
$CaO + H_2O \longrightarrow Ca(OH)_2$	−2.00	16.00	−5.71	94.12

Reaction equations in cement chemistry notation, where C = CaO, H = H_2O, S = SiO_2 [90]. Note C_3S and C_2S denote alite and belite, respectively, two major Portland clinker phases. The hydrated product, or calcium silicate hydrate (C-S-H), has been modelled using tobermorite and jennite-type endmember compositions. Volume calculations based on molar volume data from Matschei et al. [31] and Lothenbach et al. [105]. Specific to this table, V_0 and $V_{s,0}$ represent the molar volume of the reactants and its solid component, respectively (note V_0 [m^3] denotes initial sample volume in the remainder of the text).

uniform pressure conditions within the system, while the fourth represents mass transfer into the system.

For porous media like cement, the external dimensions of the system can be conveniently defined in terms of the bulk volume: $V_{ext} \equiv V_{bulk} = V_{solid} + V_{pore}$, where V_{solid} and V_{pore} [m^3] denote volume occupied by solid and pore space, respectively. Changes in bulk volume then become:

$$\Delta V_{bulk} = \Delta V_{solid} + \Delta V_{pore} \tag{3}$$

The volume change of the solid can be subdivided in:

$$\Delta V_{solid} = \Delta V_{solid}^{r(PT)} + \Delta V_{solid}^{el} + \Delta V_{solid}^{th} \tag{4}$$

Here, $\Delta V_{solid}^{r(PT)}$ [m^3] denotes the net solid volume created during reactions, ΔV_{solid}^{el} [m^3] denotes solid volume change due to elastic deformation upon mechanical loading, and ΔV_{solid}^{th} [m^3] denotes solid volume change related to thermal expansion. The pore volume change is difficult to quantify, but will include both increasing and decreasing components for CEA-modified cements. Entrapment and expansion of pores due to displacive mineral growth will contribute to the pore volume, ΔV_{pore}^{+} (>0) [m^3], while i) precipitation in the pore space, and ii) redistribution of solid due to capillary tension and mechanical compaction effects [28,86] will reduce the pore volume, ΔV_{pore}^{-} (<0) [m^3].

For the fluid phase, we can write:

$$\Delta V_{fluid} = \Delta V_{fluid}^{r(PT)} + \Delta V_{fluid}^{el} + \Delta V_{fluid}^{th} + \Delta V_{fluid}^{supply} \tag{5}$$

where $\Delta V_{fluid}^{r(PT)}$ [m^3] is the net volume of fluid consumed in reaction, ΔV_{fluid}^{el} and ΔV_{fluid}^{th} [m^3] represent elastic and thermal contributions, respectively, and $\Delta V_{fluid}^{supply}$ [m^3] denotes the volume of fluid supplied from the environment. Assuming initially saturated conditions, but allowing development of unsaturated conditions through evaporation of a small amount of pore fluid, i.e. $\Delta V_{pore} \approx \Delta V_{fluid} + \Delta V_{vapor}$, while noting that $\Delta V_{chem} = \Delta V_{solid}^{r(PT)} + \Delta V_{fluid}^{r(PT)}$, Eqs. (3)–(5) can be combined to:

$$\Delta V_{bulk} = \Delta V_{chem} + \Delta V_{solid}^{el} + \Delta V_{solid}^{th} + \Delta V_{fluid}^{el} + \Delta V_{fluid}^{th} + \Delta V_{vapor} + \Delta V_{fluid}^{supply} \tag{6}$$

$$\Delta V_{pore} \approx \Delta V_{fluid}^{r(PT)} + \Delta V_{fluid}^{el} + \Delta V_{fluid}^{th} + \Delta V_{fluid}^{supply} + \Delta V_{vapor} \tag{7}$$

Development of unsaturated conditions ($\Delta V_{vapor} > 0$) requires the pore fluid pressure to drop to its vapor or cavitation pressure, which under fixed confining pressure increases the effective stress on the porous framework of the solid cement. At this stage, note $\Delta V_{chem} < 0$ for both Portland cement and MgO hydration ($\Delta_r V^{PT}/V_0$, Table 1). Achieving bulk expansion ($\Delta V_{bulk} > 0$) using MgO-based CEAs therefore relies on the creation of pore space via displacive crystal growth ($\Delta V_{pore}^{+} > 0$), not creation of solid volume ($\Delta V_{solid}^{r(PT)}$). As stated, $\Delta V_{pore} = \Delta V_{pore}^{+} + \Delta V_{pore}^{-}$, with both the expansive (FoC-development) and compactive (capillary tension, mechanical compaction) processes depending on stress state. External fluid supply will therefore have a significant impact on MgO-based expanding cements, as inflow of fluid allows ΔV_{pore}^{+} to develop without pore fluid pressure collapse, which would otherwise enhance compactive mechanisms.

3. Experimental methods

3.1. Materials and cement sample preparation

The experiments were performed on cement slurries prepared following ISO 10426-2 [121]. The investigation included a standard Class G Portland cement (E0, Table 2), as reference system, and three expanding cements containing increasing amounts of MgO-based expansion additive (denoted E5, E10 and E20, Table 2). The series of cement slurries was designed to have constant density (1.88 g cm^{-3}) and minimal differences in the curing time and initial solid volume fraction. Cements E0 and E5 have previously been studied by Jandhyala et al. [45], who report relevant data on slurry consistency and workability. All slurries were prepared immediately prior to use, with data logging usually commencing within 20 min after mixing. The MgO material used can be classified as “hard burnt” or “medium reactive” [108]. For further details, see Supplementary information, Section S.1.1.

3.2. Apparatus description

The experiments were performed in a LABCAT apparatus (Fig. 1), which was briefly introduced by van Eijden et al. [38], but will be discussed in more detail here. This apparatus allows for concurrent measurement of the chemical shrinkage (i.e. volume change of reaction) and bulk volume change (i.e. variations in the external dimensions) that occur during the hydration and setting of cement samples. The LABCAT can be operated at 35–200 °C and total pressures of up to 40 MPa to simulate downhole conditions. Following the approach of previous studies [46,49], volume change determinations are based on the influx-efflux of water required to maintain pressure. However, the LABCAT

Table 2
Initial composition and properties of the cement slurries investigated in this study.

Cement slurry composition		E0 [g]	E5 [g]	E10 [g]	E20 [g]
Components	[g cm^{-3}]				
Tap water	1.00	44.22	46.84	49.46	54.69
Portland Class G cement	3.15	100.00	100.00	100.00	100.00
MgO-based expansion additive	3.57	0.00	5.00	10.00	20.00
Free water control agent	1.38	0.10	0.10	0.10	0.10
Dispersant	1.28	0.30	0.40	0.50	0.70
Retarder	1.25	0.08	0.10	0.12	0.12
Defoamer	0.92	0.89	0.89	0.89	0.89

Calculated cement slurry properties	E0	E5	E10	E20
Compounded slurry density (ρ_s) [g cm^{-3}]	1.88	1.88	1.88	1.88
Initial solids content (s_0) [wt%]	68.69	68.48	68.30	67.99
Initial solids content [vol%]	41.07	40.71	40.39	39.85
Initial CEA content [wt%]	0.00	3.26	6.21	11.33
Initial CEA content [vol%]	0.00	1.72	3.28	5.98

For further details on wellbore cementing additives used, see Supplementary information, Section S.1.1.

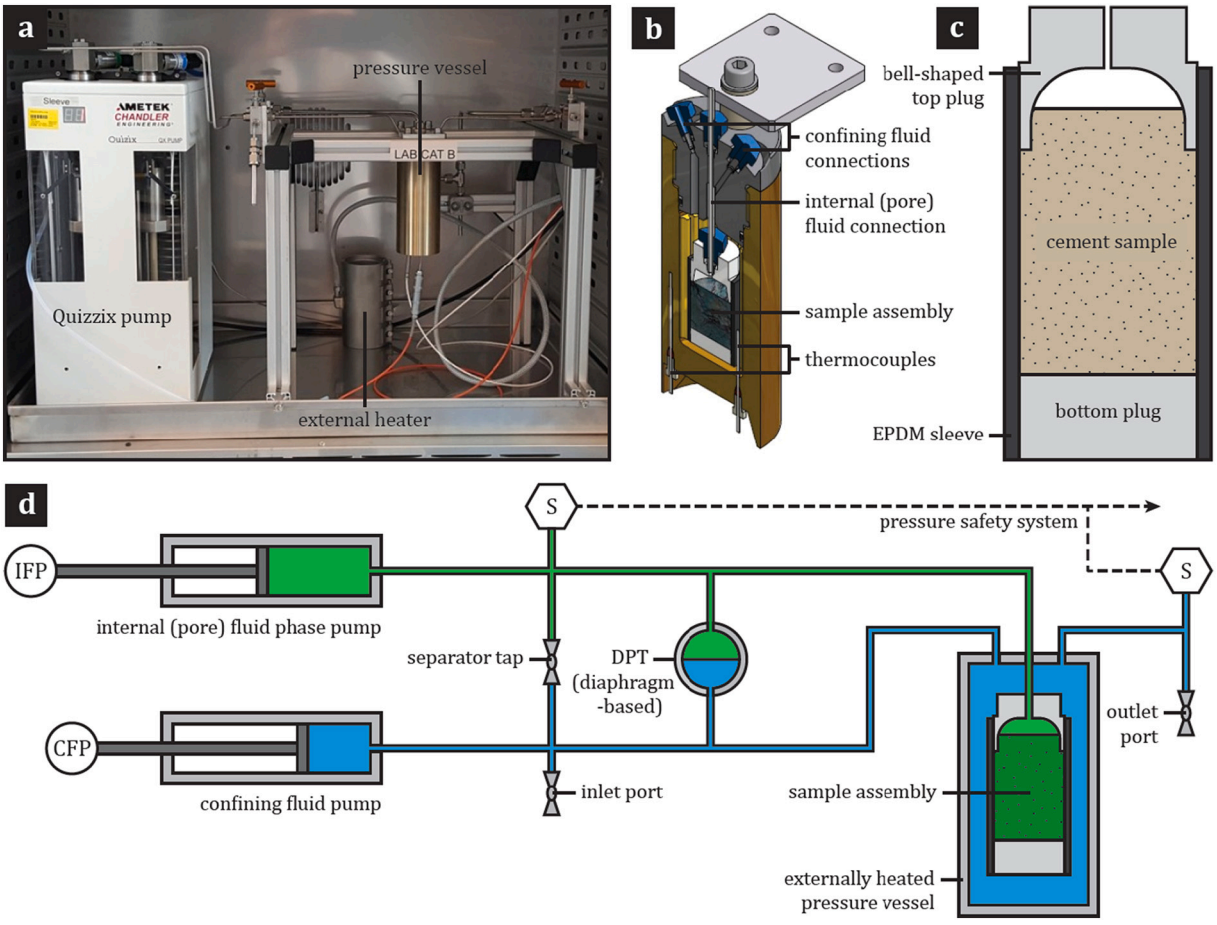

Fig. 1. Overview of the LABCAT apparatus, with a) photograph, b) cross-section of the pressure vessel, showing the sample assembly, internal fluid connection, confining fluid connections and thermocouples, c) cross-section of the sample assembly (not to scale, tourniquets not shown), and d) a schematic of the LABCAT apparatus, showing the confining fluid pump (CFP), internal (pore) fluid phase pumps (IFP), differential pressure transmitter (DPT) and separator tap. The internal (pore) fluid phase system, including the sample, is indicated in green, the confining fluid system is indicated in blue. (For interpretation of the references to colour in this figure legend, the reader is referred to the web version of this article.)

differentiates itself from earlier testing facilities in that it can measure and control both the internal (pore) fluid phase pressure and the confining pressure acting on the hydrating cement sample.

The main body of the LABCAT apparatus consists of an externally heated pressure vessel, containing the sample assembly, and a Quizix QX6000 dual cylinder high-pressure pump. One pump cylinder, hereafter referred to as the "confining fluid pump" (CFP), is used to control the confining pressure acting on the sample, P_{cf} [Pa] (Fig. 1d). The other cylinder, denoted the "internal fluid phase pump" (IFP), connects directly to the sample (Fig. 1d). The nature of this "internal fluid phase" changes over the course of an experiment. Initially, the internal fluid phase pressure, P_{if} [Pa], will reflect the hydrostatic cement slurry pressure. Later, as the cement starts to form a solid framework, capable of supporting mechanical loads, P_{if} [Pa] becomes some measure for the pore fluid pressure in the cement matrix. Pressure differences between the CFP and IFP, $\Delta P = P_{cf} - P_{if}$ [Pa], can only develop after a separator tap is closed to disconnect the two systems (Fig. 1d). This ΔP is measured directly using a differential pressure transmitter (DPT, Fig. 1d), where an initial Rosemount 3051-type DPT [38] was later replaced by a Fuji FKC-type DPT to increase the operable pressure range. Three PT-100 thermocouples are used to measure temperature, with the one in the confining fluid located closest to the sample (Fig. 1b).

The sample assembly, containing the cement slurry, consists of an EPDM sleeve (inner diameter 25 mm, length 50 mm) with a stainless-steel, solid bottom plug (height 12 mm) and bell-shaped top plug (height 20 mm), the latter fitted with an internal (pore) fluid connection (Fig. 1b). The EPDM sleeve functions as an impermeable yet deformable barrier, which conforms to bulk volume changes in the cement sample. The LABCAT is housed inside a Binder Series FED heating chamber, providing a constant temperature environment ($T_o = 35 \pm 0.1$ °C). The pressure vessel is further equipped with an electrical heater, allowing sample temperatures (T_s) of up to 200 °C to be attained.

3.3. Experimental procedures and progression

In preparation of each experiment, both cylinders of the pump were filled with degassed water, ensuring the pistons were positioned midway their operable range. To set up an experiment, 10–12 ml cement slurry (V_0 [m^3]) was placed in the sample assembly, using wire tourniquets to seal the EPDM sleeve against the plugs, while taking care that the slurry level reached some distance into the bell-shaped chamber of the top plug (Fig. 1c). This ensured settling of cement (free water-formation) would not lead to pinching of the EPDM sleeve at the cement-top plug contact. The sample assembly was then mounted in the pressure vessel, connecting the top plug to the internal fluid phase system. The LABCAT was subsequently filled with degassed water via the inlet port (Fig. 1d), using a plastic syringe. Displaced air got vented via the outlet port, which was closed once water emerged (Fig. 1d). After applying a small initial pressure (~0.5 MPa) using the syringe, the inlet port was also closed. The LABCAT was pressurized further to P_{cf} using the CFP, and brought to temperature. Throughout this process, the separator tap remained open to ensure zero effective pressure acted on the sample ($\Delta P = 0$). Stable

temperature (T_o, T_s) was attained within 1 h.

At this stage, the separator tap was closed, disconnecting the CFP and IFP subsystems (Fig. 1d). The CFP continued to maintain the confining fluid system at P_{cf}. Conversely, with the IFP remaining off, pressure in the now disconnected internal fluid phase system (P_{if}) was no longer controlled. Meanwhile, hydration was ongoing in the cement and would continue to cause chemical shrinkage. Initially, while the cement still behaved slurry-like, this shrinkage was accommodated largely by inward displacement of the EPDM sleeve, i.e. by bulk volume shrinkage. Consequently, the CFP had to deliver water to maintain pressure, while the internal fluid phase pressure remained $P_{if} \approx P_{cf}$ (see Stage I, Fig. 2). Later, as the cement started to form a load-bearing solid framework, part of the chemical shrinkage would instead get accommodated internally, e.g. by development of stresses in the solid matrix and lowering of the pore fluid pressure, with $P_{if} < P_{cf}$ (Stage II, Fig. 2). Assuming P_{if} reflects the pore fluid pressure in the cement matrix at this stage, ΔP corresponds to the Terzaghi effective confining pressure acting on the solid. Once a pre-set maximum ΔP was reached (ΔP_{lim} [Pa], Table S1), the IFP would start controlling P_{if} and prevent it from dropping any further. From this point on, internal accommodation of chemical shrinkage would be aided by direct water supply (Stage III, Fig. 2). In what will be referred to as "reaction-controlled" experiments (denoted RC, Table S1), the IFP remained off throughout the test (no Stage III).

Experiments were terminated by turning off the IFP, opening the separator tap and turning off the heater of the pressure vessel. The LABCAT apparatus was subsequently allowed to cool down to oven temperature with the CFP controlling pressure. Once sufficiently cooled down, the pressure was lowered to 1 MPa using the CFP and then removed by opening the inlet port.

3.4. Data acquisition and processing

The pump volumes, V_{CFP} and V_{IFP} [m^3], confining fluid pressure, P_{cf} [Pa], internal fluid phase pressure, P_{if} [Pa], differential pressure, ΔP [Pa], and temperature, T_s [°C], were logged every 20 s. Following Chenevert and Shrestha [49] and Jafariesfad et al. [41], data recorded during the heating and stabilisation stage of the experiments were not considered in further analysis. From an application point of view, this is reasonable because important volume changes occur mainly after the cement gelled significantly, i.e. once shrinkage can no longer be compensated by gravitational sagging of the cement column. In this context, the point of zero-volume change ($\Delta V_{CFP} = \Delta V_{IFP} = 0$), i.e. the reference state with respect to which expansion and shrinkage are determined, was selected 1 h after closing the separator tap (~2.5 h after mixing). None of the samples had developed a notable ΔP at this stage, suggesting they behaved slurry-like (Stage I, Fig. 2). The chemical shrinkage, ΔV_{chem} [m^3], and bulk volume change, ΔV_{bulk} [m^3], of the cement samples were calculated by correcting the recorded pump data for apparatus specific storage and thermal effects (see Supplementary information, Section S1.2). Following ISO 104236-5 [120] practice, the volume changes were normalised with respect to the samples' initial volume, V_0 [m^3], obtained using their initial mass (m_0 [kg], Table S1) and the calculated slurry density, ρ_s [kg m^{-3}] (Table 2).

3.5. Post-experimental analysis of the cement samples

Upon removal from the LABCAT apparatus, the cement samples were weighed and allowed to dry under ambient conditions, prior to storage. At a later stage, the samples were dried to constant weight at 105 °C, as approximate method for determining their "non-evaporable" water content [90] (see Supplementary information, Section S1.3). Four of the samples (F08, F11, F26 and F27, see Table S1) were subsequently cast in Araldite2020 epoxy resin in preparation for sectioning. This involved cutting the cylindrical samples perpendicular to their axis, at a location about midway their height, and polishing the cross-sections thus obtained using standard lapidary equipment. Sections were studied using reflected light microscopy.

4. Results and analysis

4.1. LABCAT volume and pressure data

Thirty-two LABCAT experiments have been performed, systematically varying i) the MgO-based CEA concentration (see Table 2) and ii) the maximum effective confining pressure, ΔP_{lim}, that was allowed to develop during hydration. Experiment durations varied from 4 to 38

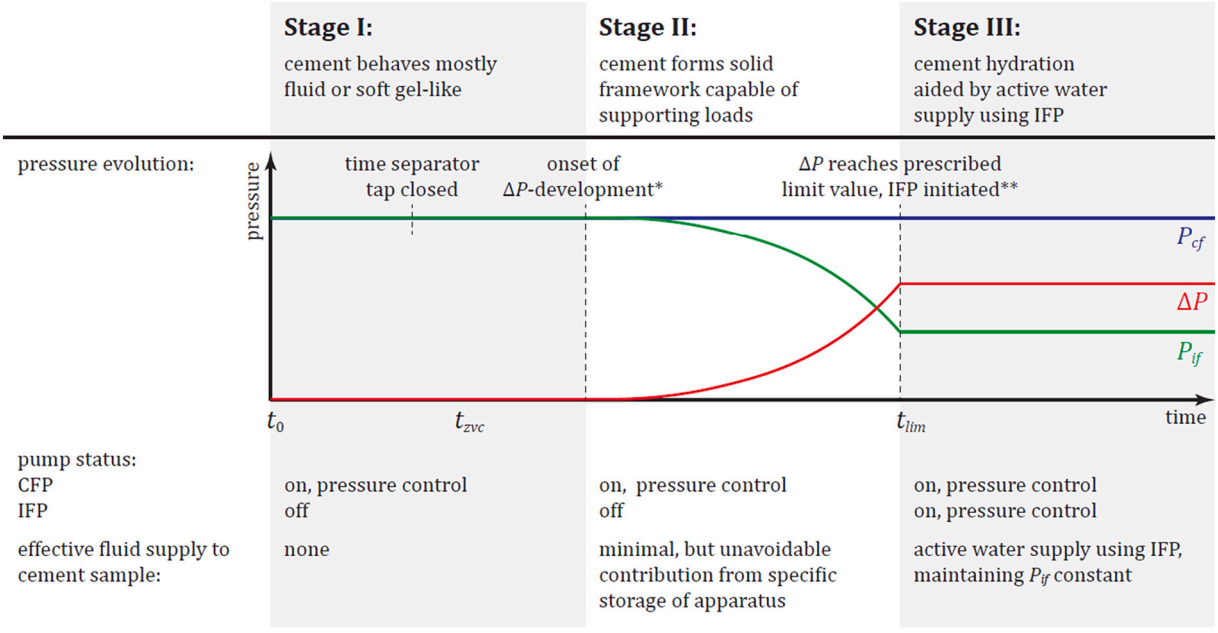

Fig. 2. Schematic representation of pressure evolution, pump status and effective fluid supply during a typical cement hydration experiment in the LABCAT. The pressure response can be divided into three stages (see Section 3.3). The transition from Stage I to II is relatively gradual, but the onset of Stage III is marked by IFP activation. The t_0, t_{zvc} and t_{lim} denote characteristic points in the evolution of the hydrating cement samples (see Section 4.1).

days. Each LABCAT experiment provided data with time on i) chemical shrinkage, $e_{chem} = \Delta V_{chem}/V_0$ [–], ii) the bulk volume change of the sample, $e_{bulk} = \Delta V_{bulk}/V_0$ [–], and iii) the pressure difference, ΔP [MPa], developed during hydration. For e_{chem} and e_{bulk}, note expansions are defined positive, while negative values denote chemical and bulk shrinkage, respectively. To facilitate analysis, several characteristic moments in the evolution of the samples were defined. With reference to the illustrations of Fig. 3, these points in time include:

- Point t_{zvc}: Predefined state of zero-volume change (see Section 3.4).
- Point t_f: Time of experiment termination.
- Point t_{min}: Moment when $e_{bulk}(t)$ attains its minimum value for $t_{zvc} < t \leq t_f$, i.e. the largest bulk volume shrinkage recorded.
- Point t_{max}: Moment when $e_{bulk}(t)$ attains its maximum value for $t_{min} < t \leq t_f$, i.e. representing possible bulk volume regained after the minimum in bulk volume was attained.
- Point t_{net0}: Moment when $e_{bulk}(t) = 0$ for $t_{min} < t \leq t_f$, i.e. the transition from net bulk shrinkage to expansion. Not all samples attained this state, some showing net bulk shrinkage throughout.
- Point t_{lim}: Moment when $\Delta P(t)$ reaches its limit value (ΔP_{lim}) for $t_{zvc} < t \leq t_f$, i.e. onset of Stage III (Fig. 2). This point is never reached in reaction-controlled experiments (denoted RC).
- Point $t_{\Delta P}$: Moment at which ΔP reaches its maximum value for $t_{zvc} < t \leq t_f$. For RC experiments, this denotes the effective confining pressure attained due to hydration and self-desiccation.
- Point t_{SII}: End of Stage II (Fig. 2). Note this corresponds to Point t_f in RC experiments and Point t_{lim} in the others.
- Point t_{chem}: Moment when $e_{chem}(t)$ attains its minimum value for $t_{ZVC} < t \leq t_f$, i.e. the largest chemical shrinkage recorded. Found to coincide with Point t_f, therefore not tabulated separately.
- Finally, various points t_{yd} register the sample properties at time $t = y$ days.

Insofar applicable, the values for e_{chem} [–], e_{bulk} [–], ΔP [bar] and t [h] at the above characteristic moments in the samples' evolution have been tabulated in Table S1. Below, the behaviour of the cement samples will be characterised further using subsets of these data.

4.1.1. General behaviour of the E0-type (non-expanding) reference cement

Fig. 4 shows the volume evolution of non-expanding (E0) cement samples in three LABCAT experiments (R01–R03) performed using progressively higher ΔP_{lim}-values. The samples showed very similar chemical shrinkage behaviour, attaining −4.04% to −4.08% after four days (t_{4d}), and about −4.1% at termination after nearly seven days (Fig. 4a). This consistency suggests the hydration reactions were not significantly affected by the stress state imposed. As expected, all non-expanding (E0) cement samples displayed bulk shrinkage. Unlike chemical shrinkage, however, bulk shrinkage varied markedly with ΔP_{lim}. In the sample hydrated under low effective confining pressure (R01, $\Delta P_{lim} = 0.2$ bar), bulk shrinkage reached −1.64%, accommodating ~40% of the chemical shrinkage. By contrast, the sample hydrated under RC conditions (R03) developed ΔP up to 10.9 bar (Fig. 4b). Note this maximum ΔP occurred around 30 h, where the subsequent lowering (i.e. increase in P_{if}) could reflect compaction of the cement matrix or minor leakage. In any case, sample R03 showed −3.94% bulk shrinkage at experiment termination, thereby accounting for ~96% of the chemical shrinkage. The difference is clearest in Fig. 4c, where the 1:1 line delineates "fluid phase behaviour", where chemical shrinkage is accommodated entirely via bulk volume change.

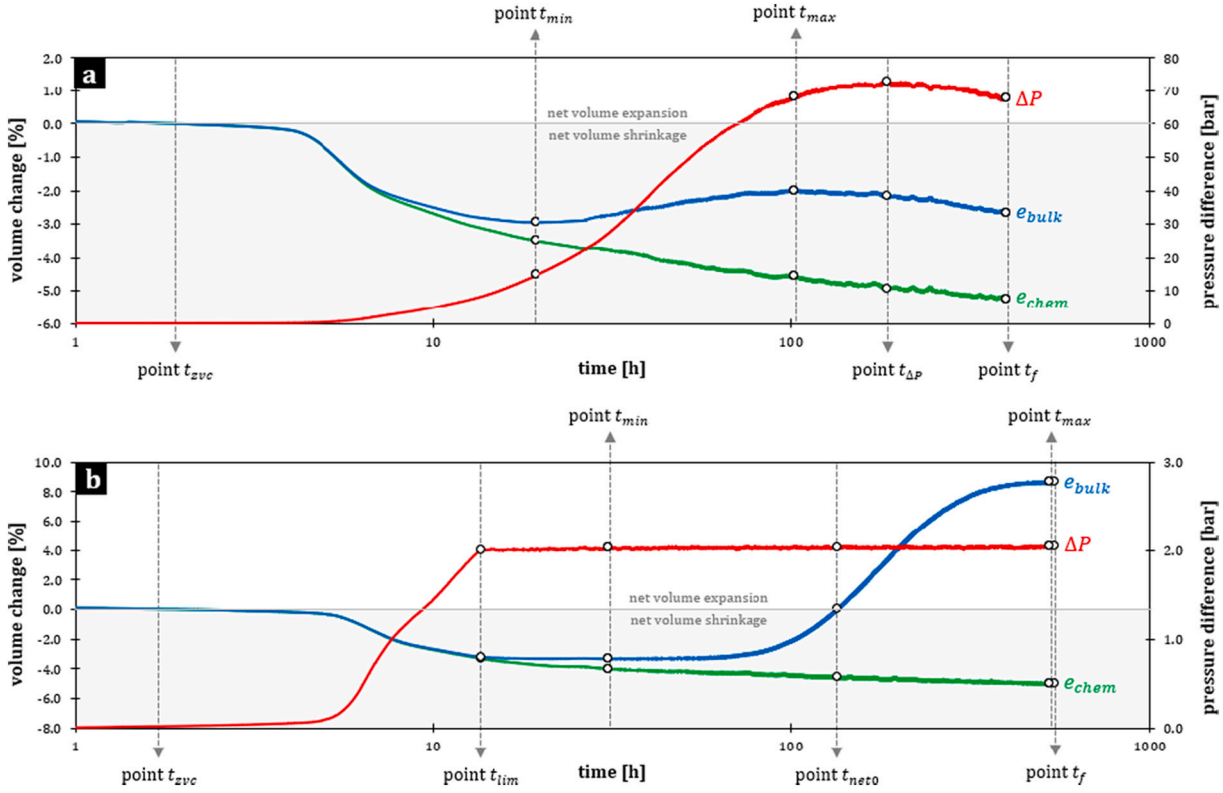

Fig. 3. Examples of $e_{chem}(t)$, $e_{bulk}(t)$ and $\Delta P(t)$ data obtained from the LABCAT, where a) and b) show F22 and F10, respectively (Table S1). Note F22 was hydrated under reaction-controlled conditions, allowing a substantial ΔP to develop (see Stage II, Fig. 2). Despite the high MgO-based CEA concentration (E20), F22 displayed net bulk volume shrinkage throughout the experiment. By contrast, F10 was hydrated under $\Delta P_{lim} = 2$ bar. This limit was reached after 13.6 h, initiating water supply (Stage III, Fig. 2). Under these conditions, a lower amount of MgO-based CEA (E5) could generate a net bulk volume expansion of ~9%. The plots further indicate a series of characteristic points in the evolution of the hydrating cement samples (t_{zvc}, t_f, t_{min}, t_{max}, t_{net0}, t_{lim} and $t_{\Delta P}$), defined to facilitate analysis and enable comparisons.

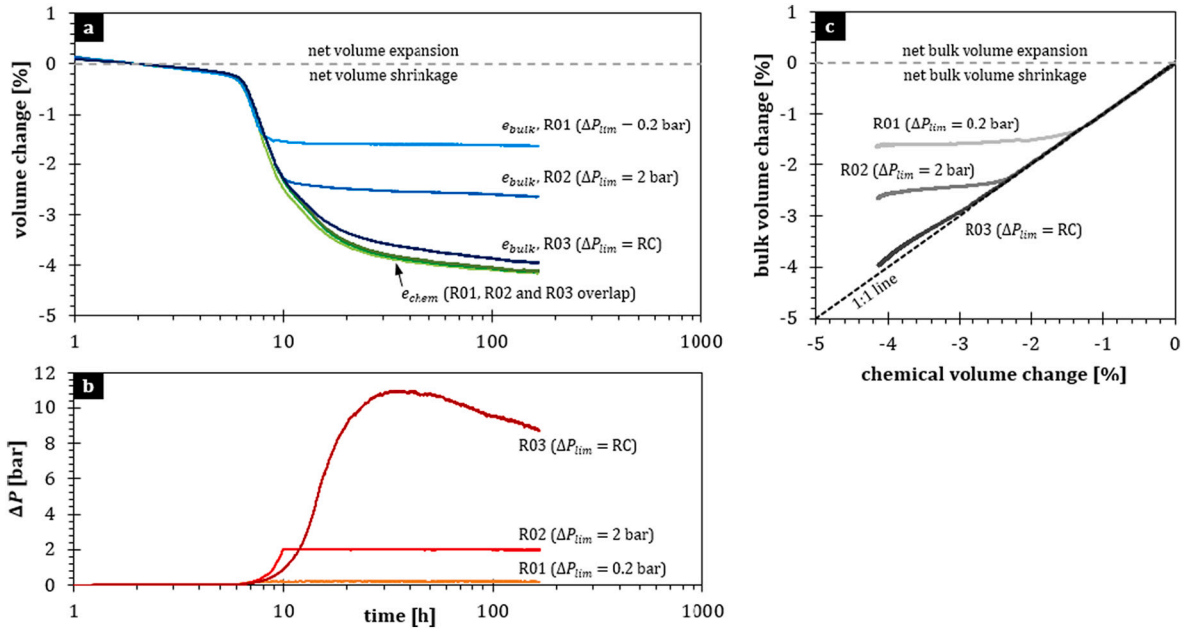

Fig. 4. Volume and pressure evolution of E0 (non-expanding) cement samples R01, R02 and R03 (Table S1), all hydrated at $P = 100$ bar, $T = 90$ °C, with: a) bulk volume change (blue) and chemical volume change (green) with time, b) pressure difference with time, and c) bulk volume change versus chemical shrinkage. (For interpretation of the references to colour in this figure legend, the reader is referred to the web version of this article.)

4.1.2. General behaviour of the expanding cements

Fig. 5 shows the volume evolution of E5-type expanding cement samples, in LABCAT experiments which allowed progressively larger ΔP to develop during cement hydration. Like the non-expanding cement, the E5 samples showed similar chemical shrinkage irrespective of ΔP_{lim}-value imposed (Fig. 5a), registering e_{chem} of −4.2% to −4.4% after four days. Addition of 5% bwoc MgO-based CEA resulted in markedly different bulk volume behaviour, producing net increases at lower ΔP_{lim}-values (F11, F10, Fig. 5a). However, this expansion-effect diminished rapidly when larger effective confining pressures were allowed to develop during hydration (F13, F12, Fig. 5a). Sample F11 (ΔP_{lim} = 0.2 bar) already showed less bulk shrinkage than E0 cement in the early stages (cf. R01, Fig. 4a), attained net zero bulk shrinkage after ~52 h, and reached a maximum bulk expansion of ~15.7% around the time of experiment termination (Fig. 5a). When a ΔP_{lim} of 2 bar was imposed (F10, Fig. 5; R07 and F03, Table S1), the largest bulk shrinkage recorded (−3.4% to −2.4%) was comparable to that in E0 cement (cf. R02, Fig. 4a). After this initial period of bulk shrinkage, the E5 samples began to expand, attaining net zero bulk shrinkage after 98 to 135 h (F10, R07 and F03, Table S1). Sample F10 reached a bulk expansion of 8.6% (Fig. 5a). By contrast, samples hydrated under higher ΔP_{lim}-values of 15–20 bar (F13 in Fig. 5; F08 and R10, Table S1) generally showed less

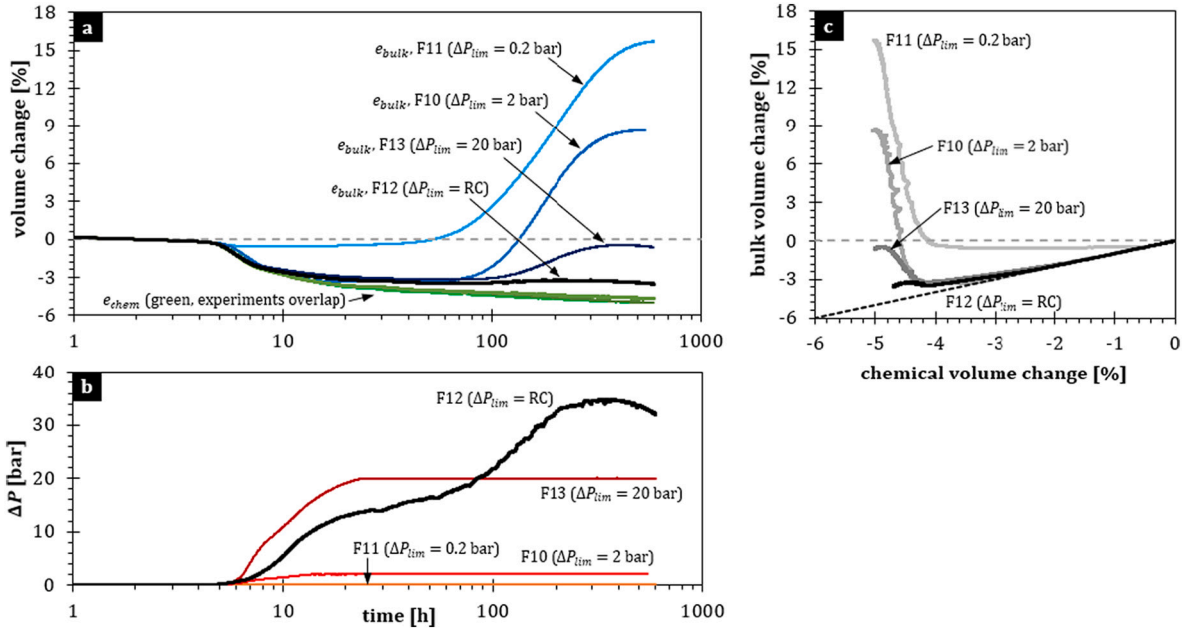

Fig. 5. Volume and pressure evolution of E5 expanding cement samples F10, F11, F12 and F13 (Table S1), with a) bulk volume change (blue) and chemical volume change (green) with time, b) pressure difference with time, and c) bulk volume change versus chemical shrinkage. (For interpretation of the references to colour in this figure legend, the reader is referred to the web version of this article.)

bulk shrinkage than their E0-cement counterparts, but never reached net bulk expansion. Under reaction-controlled (RC) conditions (F12, Fig. 5; R11, Table S1), differential pressures of up to 34.8 bar were developed (Fig. 5b), while bulk volume increases were very limited, reaching −3.5% to −4.1% net bulk volume change, compared to −4.6% chemical shrinkage. Most bulk volume expansion occurs at $e_{chem} < -3\%$, i.e. relatively late in the hydration history, regardless of ΔP_{lim}-value (Fig. 5c). The E10 and E20 cements behaved essentially similar to the E5 samples (Figs. S2 and S3). The amount of bulk volume expansion achieved increased with MgO content, but remained very limited under reaction-controlled (RC) conditions, even at the highest concentration tested (compare F12, Fig. 5a and F16, F22, Fig. S3a).

4.1.3. Effect of expansion additive concentration on chemical volume change

Fig. 6 plots e_{chem} [–] versus ΔP [bar] for various characteristic points in the samples' evolution. Cement type (E0–E20, Table 2) is indicated using colour. Chemical shrinkage generally increased with higher MgO-based expansion additive concentrations (e.g. Fig. 6h). This trend with cement composition is likely due to the large negative volume change of reaction associated with MgO hydration (~15% volume decrease, Table 1), which can contribute significantly to overall chemical shrinkage of the sample (Supplementary information, Section S2.1.2). Cements hydrated under different ΔP_{lim}-values at first glance displayed similar chemical shrinkage (Figs. 4–5, S2–S3). However, in the e_{chem} [–] versus ΔP [bar] data, samples hydrated under low effective confining pressures showed slightly more chemical shrinkage than those hydrated under higher confinement (Fig. 6a–d). Despite considerable scatter, this trend seems quite systematic with time and occurred at several additive concentrations.

4.1.4. Effect of expansion additive concentration on bulk volume change

Fig. 7 shows the bulk and chemical volume evolution of E5, E10 and E20 cement samples hydrated with $\Delta P_{lim} = 2$ bar (Fig. 7b). Under these low confinement conditions, increasing the CEA concentration from 5% bwoc (F10) to 10% bwoc (F26) resulted in an earlier onset of bulk expansion (e.g. t_{net0} is reached at ~135 h for F10, ~40 h for F26) and larger bulk expansion values (Fig. 7a). Increasing the CEA concentration to 20% bwoc (F14) had little effect on earliest-stage behaviour, but led to somewhat larger bulk expansion values overall (Fig. 7a). No clear trends with CEA concentration emerged by plotting e_{bulk} versus e_{chem}, but some extent of hydration seems required before bulk expansion could accelerate (note upshoot in e_{bulk} occurs at $e_{chem} \leq -3.5\%$, Fig. 7c). Under higher maximum effective confining pressures ($\Delta P_{lim} = 20$ bar), the impact of MgO-based CEA concentration is essentially similar (Fig. S5), but the amount of bulk expansion exhibited was generally reduced. Note that E5 cement, which produced 8.63% net bulk volume gain at $\Delta P_{lim} = 2$ bar (F10, Fig. 7a), never attained a state of net bulk volume expansion at $\Delta P_{lim} = 20$ bar (Fig. S5a).

None of the cement samples hydrated under reaction-controlled conditions showed net bulk expansion (Fig. 8a). It seems the samples showed bulk shrinkage during the early stages of hydration ($e_{chem} > -3\%$), then experienced a transient period of relative bulk volume increase, but ultimately showed continued net bulk shrinkage (Fig. 8c). This late-stage bulk shrinkage might be related to mechanical compaction of the cement matrix, e.g. caused by the effective confining pressure developed during reaction. Hydration of E20 cement yielded ΔP up to 72.6 bar (F22, Fig. 8b). In general, the effective confining pressures developed increased markedly with increasing CEA concentration (Fig. S6). This could be due to the general increase in chemical shrinkage with CEA concentration (Fig. S4), but may also reflect pore fluid pressure collapse due to enhanced internal accommodation ($\Delta V^{+}_{pore} > 0$).

Fig. 9 plots e_{bulk} [–] versus ΔP [bar] for a number of the characteristic points in the samples' evolution. Bulk volume gain increased with CEA concentration and hydration time, while the development of effective confining pressure (ΔP) clearly inhibited bulk volume increase (Fig. 9a–d). All expanding cements showed a transition from net bulk volume expansion at low ΔP to net shrinkage at higher ΔP. This transition occurred at ~15 bar in the E5 cement (Fig. 9f). Note that none of the samples tested showed net bulk expansion at the end of Stage II (Fig. 9g). In fact, in most cases, the situation at the end of Stage II approached the largest bulk shrinkage observed (cf. Fig. 9e; see also Fig. S7). This demonstrates that most of the bulk expansion was achieved only after initiation of the IFP pump, i.e. in Stage III (Fig. 2), during which the

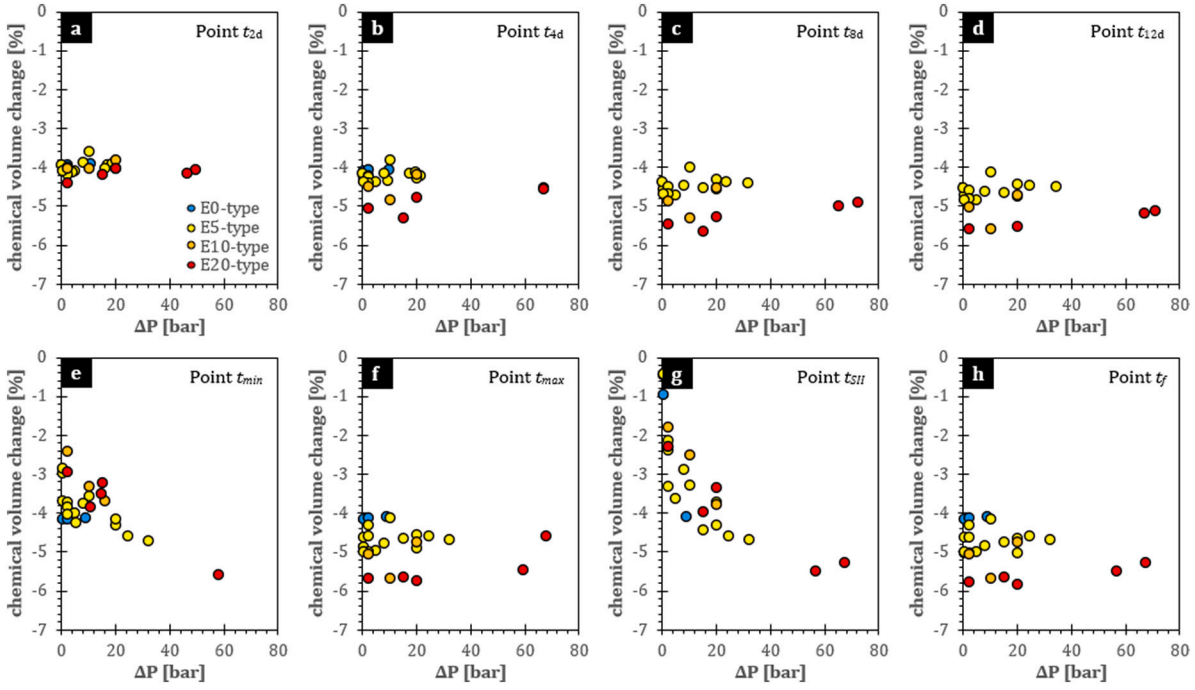

Fig. 6. Plots of e_{chem} [–] versus ΔP [bar] at various characteristic points in the evolution of the cement samples, with data shown for a–d) points t_{2d}, t_{4d}, t_{8d} and t_{12d}, respectively, e) point t_{min}, f) point t_{max}, g) point t_{SII} and h) point t_f.

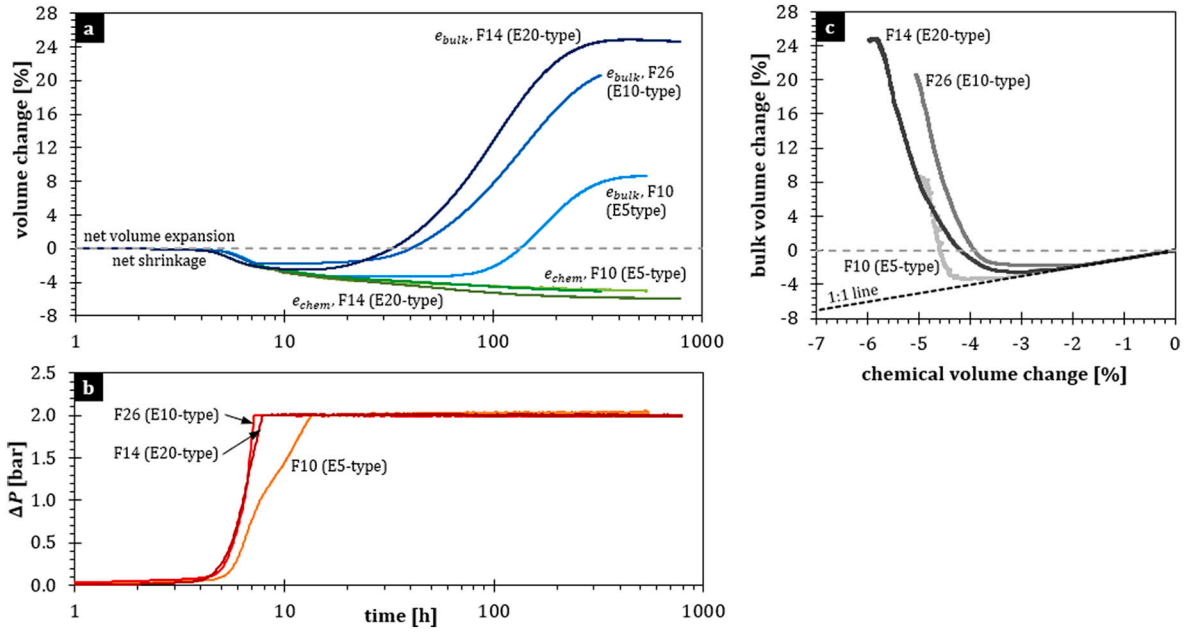

Fig. 7. Volume and pressure evolution of expanding cement samples hydrated at $\Delta P_{lim} = 2$ bar, where the MgO-based CEA concentration is systematically increased. Plots show a) bulk volume change (blue) and chemical volume change (green) with time, b) pressure difference with time, and c) bulk volume change versus chemical shrinkage. (For interpretation of the references to colour in this figure legend, the reader is referred to the web version of this article.)

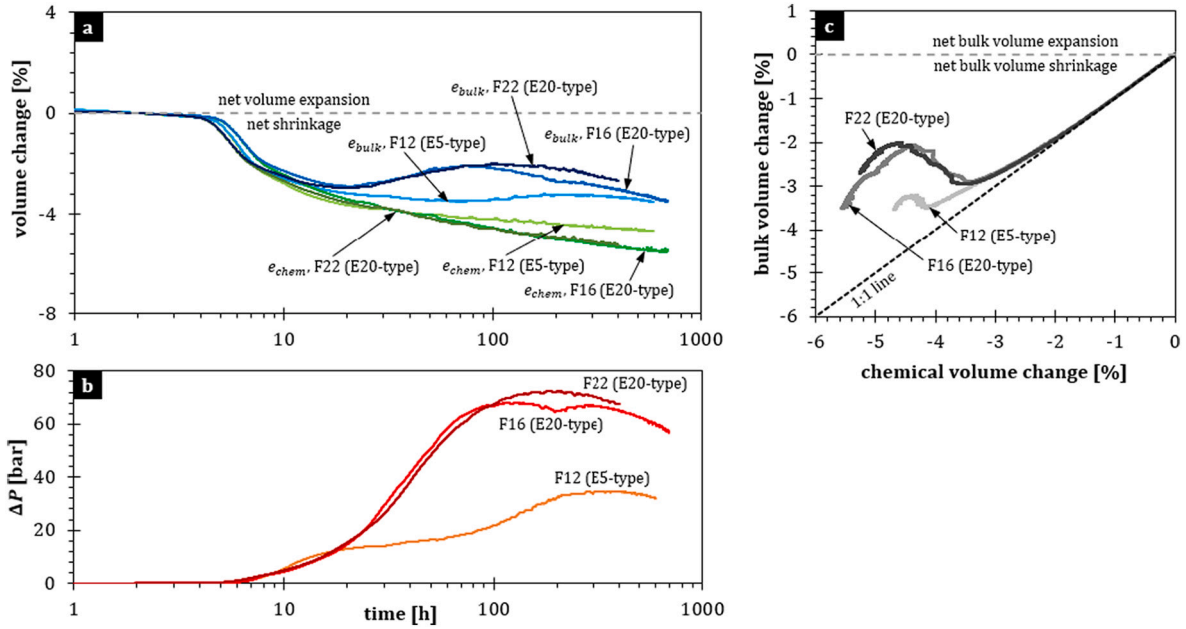

Fig. 8. Volume and pressure evolution of expanding cement samples hydrated under reaction-controlled conditions, where the CEA concentration is systematically increased. Plots show a) bulk volume change (blue) and chemical volume change (green) with time, b) pressure difference with time, and c) bulk volume change versus chemical shrinkage. (For interpretation of the references to colour in this figure legend, the reader is referred to the web version of this article.)

hydrating cement samples were mechanically supported by a constant internal (pore) fluid phase pressure (Fig. 9f).

4.2. Post-experimental and microstructural observations

Upon retrieval from the LABCAT apparatus and sample assembly, the cement samples generally emerged as cohesive objects. In a few cases, the uppermost part of the sample, which extended into the bell-shaped top plug of the sample assembly, broke off during retrieval. Otherwise, all of the samples appeared smooth and free of cracks upon visual inspection. Final sample mass and mass after heating to 105 °C have been tabulated in Table S1 and the results are discussed in the Supplementary information (Section S2.2.1). After drying, the samples developed a thin layer of white efflorescence and longitudinal striations on their surface. Samples hydrated under low confinement attained clearly larger diameters than those hydrated under higher ΔP_{lim}-values (Fig. S9). Hydration under reaction-controlled conditions resulted in somewhat concave-shaped samples. Microcracking was observed in cement samples that contained high CEA concentrations and were hydrated under low confinement, and occurred mainly along the samples'

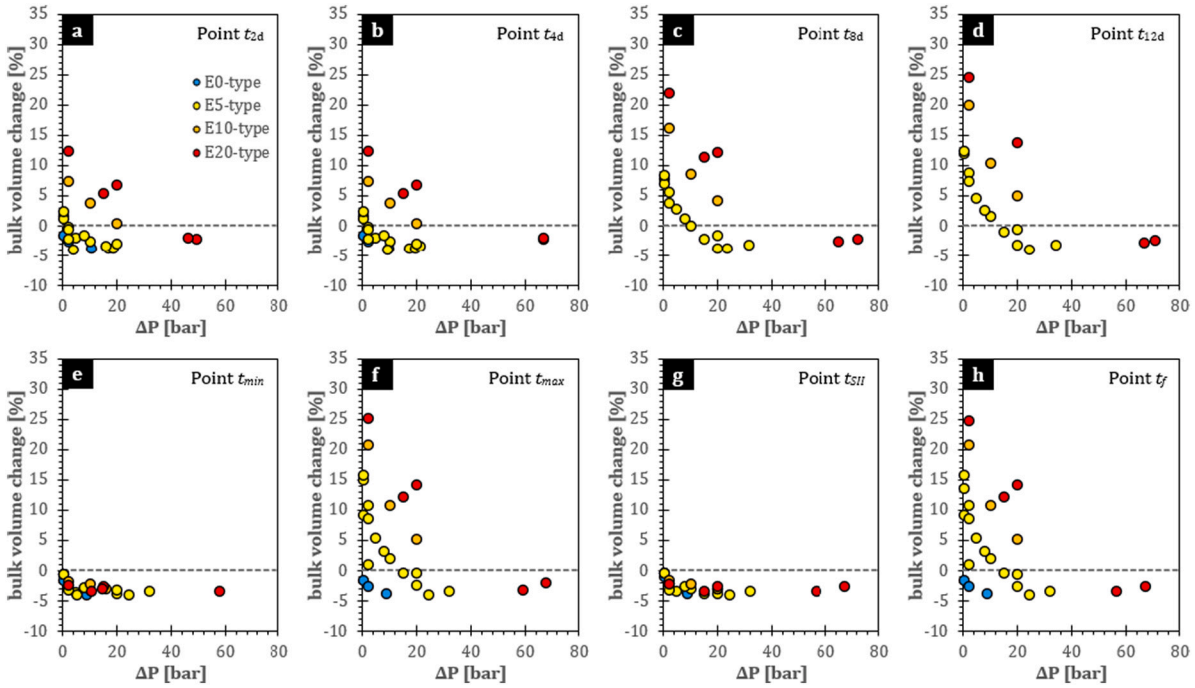

Fig. 9. Plots of e_{bulk} [–] versus ΔP [bar] at various characteristic points in the evolution of the cement samples, with data shown for a–d) points t_{2d}, t_{4d}, t_{8d} and t_{12d}, respectively, e) point t_{min}, f) point t_{max}, g) point t_{SII} and h) point t_f.

circumference (Fig. S9). It is unclear to what extent these microcracks were caused by expansive MgO hydration, as they could (partially) be due to the drying treatment at 105 °C (note the absence of visual damage upon sample retrieval and the formation of longitudinal striations upon drying). More detailed descriptions of sample microstructures are provided in Supplementary information, Section S2.2.2.

5. Discussion

Four different cement systems, containing increasing concentrations of MgO-based CEA (Table 2), were hydrated under a range of effective confining pressure conditions. The experiments showed that: i) bulk shrinkage in non-expanding cement increases with higher effective confining pressures or, equivalently, with delayed or limited access to an external water supply, ii) use of MgO-based CEAs (5–20% bwoc) produces a significant bulk expansion-effect, but this effect diminishes markedly with application of higher effective confining pressures or delayed water supply; iii) under low effective confining pressures (0.2–2 bar), MgO can create excessive bulk expansions (>5%, Fig. 9), which results in extensive microcracking. However, iv) the bulk volume gained decreases rapidly with higher confinement (>10 bar) and no net bulk expansion could be achieved under reaction-controlled conditions, i.e. without external water supply (Fig. 9); v) chemical shrinkage increased with MgO concentration. Below, we will first compare the LABCAT to conventional methods for measuring cement volume change, then discuss the effectiveness of MgO-based CEAs under various downhole situations, and finally consider the implications for wellbore cementing and zonal isolation.

5.1. Comparison with pressurized membrane and autoclave-type tests

Bulk volume change in wellbore cements has been extensively studied [25,37,40,45–55], yielding standard protocols for its measurement under atmospheric pressure conditions [120,121]. In annular ring/cylinder tests, cement is cured under free access to water, inside a spring-loaded, split ring, allowing measurement of linear expansion by monitoring the span of the split [37,53,120]. In membrane tests, cement is cured without external water access, inside an impermeable balloon, monitoring bulk volume change through Archimedes' principle [37,120]. Both methods can be modified for pressurized conditions [37,122], though the annular ring test typically requires periodic depressurization to monitor the span. Quantifying chemical shrinkage conventionally involves measurement of the water uptake by a thin layer of water-submerged cement, either in a flask [30,123] or pressure vessel [37].

The E0 and E5 cement (Table 2) were studied previously by Jandhyala et al. [45], who performed autoclave and membrane tests, respectively, to determine chemical shrinkage and bulk volume change at 1500 psi (~103.5 bar) and 190 °F (~88 °C). Bulk volume change in the membrane tests corresponded closely to observations in LABCAT experiments performed under reaction-controlled conditions (see Fig. 11 of Jandhyala et al. [45]). This corroborates the LABCAT closely approximates "closed-system" behaviour, despite inevitable inflow due to machine specific storage (Supplementary information, Section S1.2.3). Similarly, the LABCAT was able to reproduce the chemical shrinkage measured in autoclave tests, by imposing a ΔP_{lim} of 0.2 bar (see Fig. 10 of Jandhyala et al. [45]). Limiting the LABCAT pressure difference to this low value, pore fluid supply (Stage III, Fig. 2) is initiated very early on in the hydration history, approaching "fully open" boundary conditions. These comparisons provide confidence the LABCAT can simulate a range of conditions, varying from almost fully open to almost fully closed with respect to external water supply.

Jandhyala et al. [45] further investigated the effect of total confining pressure, P_{cf} [Pa], on the bulk volume response of E5 cement in membrane tests. When hydrated under $P_{cf} \approx 103.5$ bar, they observed ~4% bulk shrinkage after 12 days. Conversely, when hydrated under $P_{cf} \approx 6.9$ bar, E5 cement was able to attain ~4% net bulk expansion in 12 days (see Fig. 15 of Jandhyala et al. [45]). Interestingly, the bulk expansion observed in membrane tests under $P_{cf} \approx 6.9$ bar matches closely with the trend of e_{bulk} versus ΔP found for E5 cement in the LABCAT experiments performed under $P_{cf} = 100$ bar (Fig. 10). Unfortunately, the internal fluid phase pressure (P_{if}) cannot be measured in membrane tests, preventing direct comparison. However, since $\Delta P = P_{cf} - P_{if}$, effective stress development was probably limited by the low confining pressure ($P_{cf} \approx$

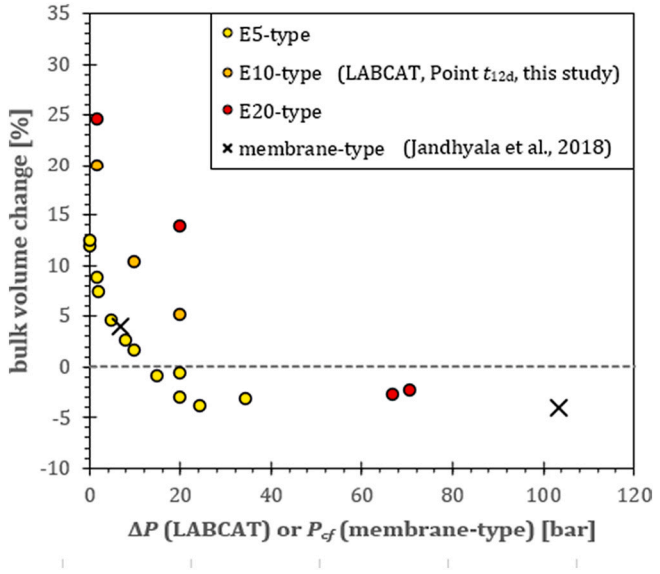

Fig. 10. Plot of e_{bulk} [–] versus ΔP [bar] after 12 days in the LABCAT experiments (circles) with e_{bulk} [–] versus P_{cf} [bar] for E5 cement after 12 days in membrane tests by Jandhyala et al. [45]. The membrane test result for $P_{cf} = 6.9$ bar corresponds well with the trend for E5 cement found in the LABCAT experiments at $P_{cf} = 100$ bar.

6.9 bar), assuming P_{if} decreased to the vapor pressure of the pore fluid. For the membrane test at $P_{cf} \approx 103.5$ bar, the ΔP-value attained remains indeterminable, but the bulk shrinkage corresponds well to that observed in LABCAT experiments performed under $P_{cf} = 100$ bar and reaction-controlled conditions, which developed ΔP of 25–35 bar. The impact of effective confining pressure on bulk volume change is seemingly independent of whether the stress state was attained under closed (membrane test at $P_{cf} \approx 6.9$ bar) or open (LABCAT at $P_{cf} = 100$ bar, $\Delta P \approx$ 6.9 bar) conditions with respect to external fluid access. This suggests that external water supply predominantly acts to provide mechanical support during hydration, rather than to replenish water as a chemical reactant.

5.2. Effectiveness of MgO-based CEAs under intermediate fluid access conditions

Volume change measured in the LABCAT for a given ΔP_{lim}-value may be used to predict the bulk response in membrane tests performed under a confining pressure equal to the pressure difference limit (Fig. 10). However, ΔP_{lim} can also be interpreted as the extent to which external fluids can imbibe and mechanically support the cement during hydration. To facilitate the analysis of cement volume change under conditions where fluid supply is allowed to varying degrees, we define a bulk expansion factor, B [–]:

$$B = 1 - \frac{e_{bulk}}{e_{chem}} \tag{8}$$

When $e_{bulk} = e_{chem}$, i.e. if all chemical shrinkage is accommodated as bulk shrinkage, $B = 0$. For situations of zero net bulk volume change, $B = 1$. Values of $B > 1$ indicate net bulk volume gain, i.e. scenarios where dilatation due to displacive crystal growth outstrips compaction due to capillary tension and creep processes activated by chemical shrinkage [25,28,29]. Note B scales with e_{chem}, taking into account the increase in chemical shrinkage with increasing MgO-concentration (Fig. S4).

In addition, we define a pore fluid depletion factor, X_p [–]:

$$X_p = \frac{\Delta P}{\Delta P_{rc}} \tag{9}$$

where ΔP_{rc} is the maximum pressure difference that develops during hydration under reaction-controlled conditions (ΔP_{max} of experiments R03, F12 and F22 were used to characterise E0, E5 and E20 cement, respectively; Table S1). Note this fluid depletion factor provides a measure for the degree of external fluid access during cement hydration. For completely unrestricted fluid supply, $X_p = 0$, as water consumed by hydration reactions would be replenished continuously, preventing pore fluid pressure decrease ($\Delta P = 0$). Conversely, $X_p = 1$ represents the drawdown that occurs during cement hydration under (nearly) zero inflow conditions, as measured in the reaction-controlled experiments ($\Delta P = \Delta P_{rc}$).

Fig. 11 shows B versus X_p reached during the hydration of E0, E5 and E20 cement (plotted Point t_{max} data, Table S1). For both the reference and MgO-based expanding cements, the variation in bulk volume response observed with degree of external fluid access can be described reasonably well using exponential relationships. Non-expanding (E0) cement shows net bulk shrinkage ($B < 1$), even at very low degrees of pore fluid pressure depletion (at $X_p = 0$, predicted $B = 0.66$), i.e. regardless of whether external fluids can imbibe the cement. Adding 5% bwoc MgO-based CEA results in net bulk volume expansion at $X_p < 0.5$, while at higher pore fluid pressure depletion factors, $B < 1$. This implies E5 cement expands over a limited range of hydrodynamic conditions only, as some inflow of external fluid seems to be required. The overall trend with X_p remains comparable, noting the exponential factor is 2.7–2.8 for all three cements (Fig. 11). Increasing the CEA concentration to 20% bwoc extends the X_p-range over which $B > 1$, though the additional volume gained is less than the effect achieved by adding the first 5% of CEA. Note that net bulk volume expansion could was not achieved in experiments where external fluid access was highly restricted ($X_p >$ 0.8), regardless of CEA concentration used (Fig. 11).

5.3. Estimated porosity trends

The exponential trends in Fig. 11 are qualitatively reminiscent of the porosity-effective stress relations encountered in a range of compaction processes, including geological basin development [124,125], sintering of porous metals [126,127] and the confined stress-strain-hydration behaviour of precompacted CaO powder aggregates (see Fig. 11 of Wolterbeek et al. [86]). Unfortunately, defining a suitable reference state/porosity is challenging for the case of cement hydration, as cement

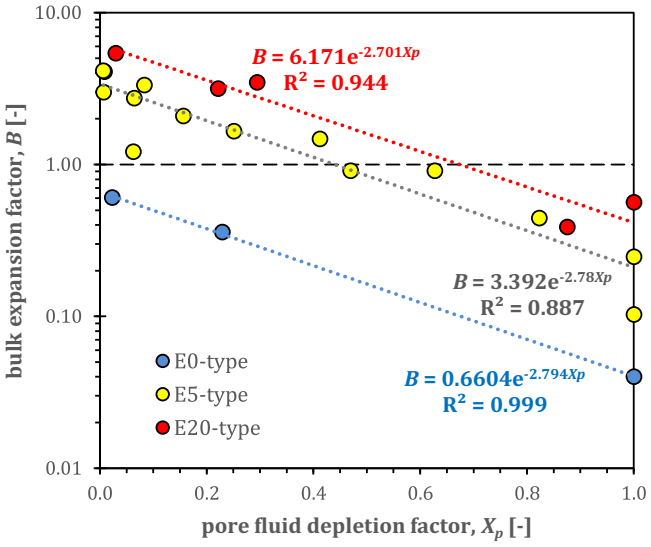

Fig. 11. Bulk expansion factor, B [–], versus pore fluid depletion factor, X_p [–], at point t_{max} in various LABCAT experiments on E0, E5 and E20 cements. The black dashed line represents zero net bulk volume change (no shrinkage, nor expansion). Dotted lines and equations denote exponential fits to the data.

slurries start out as suspensions (Table 2). However, it is possible to estimate and track the "porosity" of the samples, defined as $\varphi = 1 - s$ [–], where s [–] is the solid volume fraction, by determining solid produced via hydration. Assuming the net solid volume created (products minus reactants) is proportional to the chemical shrinkage, $\Delta V_{solid}^{r(PT)} = \alpha V_0 e_{chem}$ (i.e. assuming the x different cement hydration reactions together produce a constant volume change of reaction):

$$\varphi = 1 - s = 1 - \frac{V_{solid}}{V_{bulk}} = 1 - \frac{s_0 + \alpha e_{chem}}{1 + e_{bulk}} \quad (10)$$

where s_0 denotes initial solid volume fraction (Table 2) and α [–] is related to the ratio of volume changes of reaction occurring in the solid and fluid phases. Assuming a net solid volume increase of 80% for cement hydration (cf. $\Delta_r V_s^{PT}/V_{s,0}$-values in Table 1), and taking the $\Delta_r V_s^{PT}/V_{s,0}$ of MgO for CEA hydration (Table 1), use of a mixing model for the chemical shrinkage (Supplementary information, Section S2.1.2) yields $\alpha_{E0} = -8.01 \times 10^{-2}$, $\alpha_{E5} = -7.29 \times 10^{-2}$, $\alpha_{E10} = -6.75 \times 10^{-2}$ and $\alpha_{E20} = -6.01 \times 10^{-2}$. Using these values in Eq. (10), the porosity evolution of the samples can be estimated from the bulk and chemical volume change data (Fig. 12).

While the porosity data are estimates only, some interesting observations can be made. Porosity changes in the three E0 cement samples, hydrated under different effective confining pressures, are very similar (Figs. 4 and 12a), with the overall reduction dominating behaviour, though porosity decreases slightly with increasing confinement (inset Fig. 12a). This suggests porosity reduction may be largely attributed to hydration, e.g. reaction products filling up pores, with mechanical compaction playing a comparatively minor role. For the E5 and E20 cements, note that samples hydrated under reaction-controlled conditions show continuous porosity decrease (Fig. 12b–c), even though the bulk volume showed transient periods of relative expansion (Fig. 8c). Under lower confinement, E5 and E20 cement show significant porosity increases after ~30 h, attaining φ of 30–40%. This suggests entrapment and expansion of pores due to displacive mineral growth exceeded pore volume reduction due to infilling and compactive mechanisms. Overall, porosity increased with CEA concentration and decreased with effective confining pressure (Fig. 12d). Further research is needed to elucidate and quantify the underlying processes. In practice, however, the forces developed seem to be limited by the strength of the cement matrix (Fig. 10), rather than the maximum FoC predicted by thermodynamic models [77,86].

5.4. Implications for wellbore cementing and zonal isolation

The LABCAT results demonstrate that FoC-based CEAs' ability to achieve bulk volume expansion depends strongly on environmental conditions, including the i) confining pressure and ii) extent to which fluids can imbibe and mechanically support the cement during hydration. This implies that the volumetric response of expanding cement juxtaposed against a permeable, water-bearing rock formation will be substantially different from that of the same cement placed inside an impermeable casing pipe.

Even cements containing large quantities of MgO (20% bwoc) seem unable to achieve net bulk expansion effectively in the absence of external fluid supply ($X_p > 0.8$, Fig. 11). When considering the implications for internal cement plugs, however, it should be noted that the trends in Fig. 11 were obtained under pressure-controlled boundary conditions, i.e. the LABCAT samples were continuously in contact with an EPDM sleeve. By contrast, bulk shrinkage of a cement plug would lead to debonding (unlike the EPDM sleeve, casing pipe does not move inward), creating pathways for ingress of external fluids, which in turn could limit shrinkage. Given this complex interplay, it is difficult to predict the actual volume response.

If external fluids are readily available, the LABCAT experiments

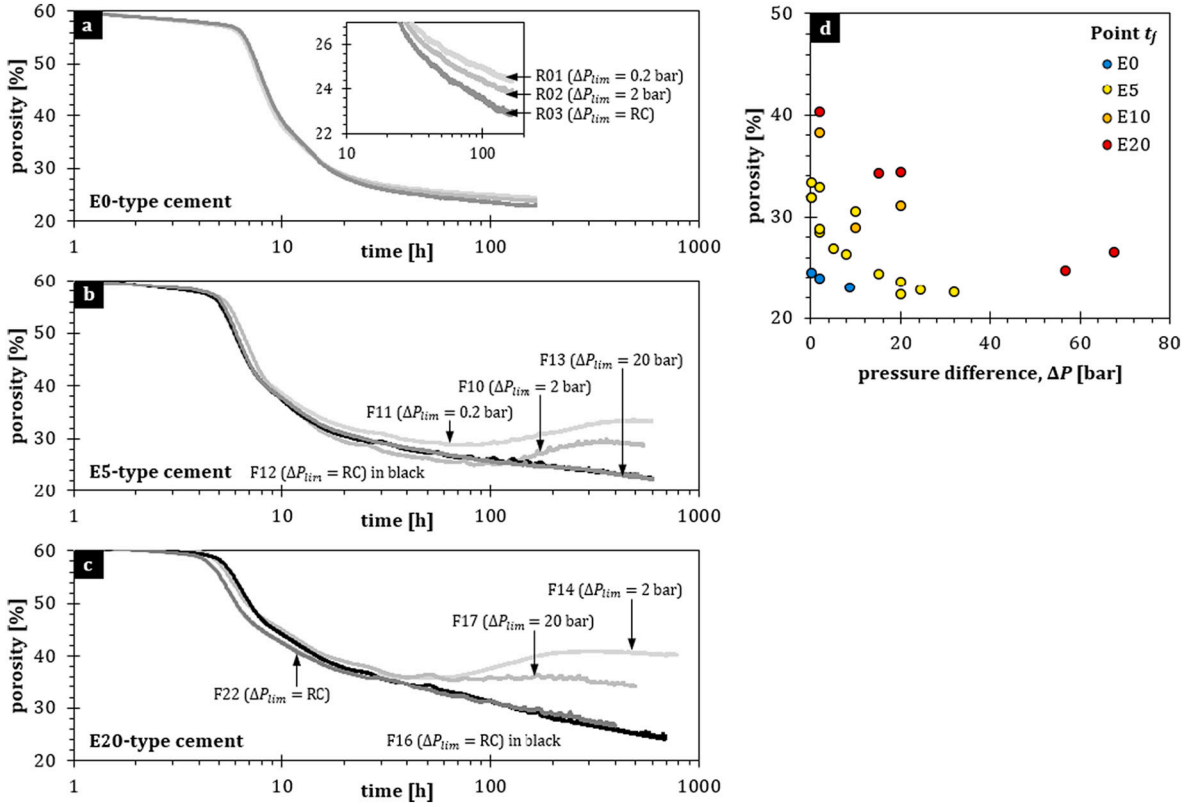

Fig. 12. Calculated porosity evolution during cement hydration in the LABCAT apparatus, with a) E0 (non-expanding) cement (see Fig. 4 for corresponding chemical shrinkage, bulk volume change and pressure data), b) E5 cement (Fig. 5), and c) E20 cement (Fig. S3); plot d) shows calculated porosity versus pressure difference at the time of experiment termination for all samples.

predict excessive bulk expansions when high CEA concentrations are used (up to 25% for E20 cement, Fig. 9f), though the amount of expansion decreases rapidly with more limited supply (Fig. 11). Again, it is important to realise the experiments were performed under pressure-controlled boundary conditions. Especially at low ΔP, this setup allows basically unrestrained expansion up to large strains. In realistic downhole scenarios, the achievable stress-bulk strain response will be controlled by the stiffness of surrounding rock formations, which provide restraints to limit free expansion [52]. Bulk expansion lessens with confinement (Fig. 10). Nevertheless, the microcracks observed in some of the samples (Fig. S9) suggest excessive expansion could have deleterious effects on cement matrix permeability. Further research is needed to assess the nature of these microcracks, as the current samples were at least partially affected by drying (Supplementary information, Section S2.2.2). Note possible microcrack development in internal plugs of E5 and E10 cement did not measurably enhance the plugs' effective permeability in sealing performance assessments [38]. The expanding cements performed significantly better compared to conventional, non-expanding cement.

The impact of heat release during hydration could not be assessed in the LABCAT experiments, but will be relevant for actual wellbore applications. Depending on reaction kinetics and the dimensions of the cement body, the heat released by cement and MgO hydration can result in significant temperature rises [2,128]. Such thermal effects were very minor in the small LABCAT samples (Supplementary information, Section S1.2.2). However, given its relevance in larger cement volumes, e.g. internal plugs, further research is needed to assess the impact of heat release during hydration. Note deleterious effects of autogenous shrinkage could be compounded by thermal shrinkage upon subsequent cooling of the hardened cement. Given the strong effect of external fluid supply in the LABCAT, we infer that slower hydrating cements may display improved expansion properties, as this would i) allow more time for fluid ingress and ii) help limit possible thermal effects.

6. Conclusions

Autogenous or bulk volume shrinkage of Portland cements is regarded one of the key factors contributing to impairment of zonal isolation along wells. Cement expansion additives (CEAs) based on force of crystallisation (FoC)-producing reactions, such as MgO hydration, mitigate autogenous shrinkage by creating internal porosity through displacive mineral growth-processes. However, both the stress-strain-reaction behaviour of CEAs and mechanisms underlying autogenous shrinkage depend strongly on stress state. Evaluation of CEA performance therefore requires measurement under representative conditions. This study provides detailed descriptions of the so-called LABCAT apparatus [38]. Using this bespoke setup, we simultaneously measured the chemical and bulk volume change of cement hydrating under downhole temperature (90 °C) and confining pressure (100 bar), while varying i) the degree of external fluid access and ii) the effective confining pressure allowed to develop due to self-desiccation. The study included a non-expanding reference cement (denoted E0) and a series of MgO-based expanding cements with CEA concentrations ranging from 5% to 20% by weight of cement (bwoc; denoted E5-E20, respectively). Based on the findings, the following conclusions can be drawn:

- If the LABCAT is programmed to mimic fluid-access conditions imposed in conventional laboratory tests for the evaluation of cement volume change (autoclave and membrane experiments), it accurately reproduces the chemical and bulk volume responses seen in such experiments. This consistency provides confidence the LABCAT yields representative volume data. However, where conventional tests impose either fully open or closed boundary conditions, the LABCAT is capable of simulating intermediate degrees of external fluid access. This enables direct exploration of the impact of fluid-access, self-desiccation and self-confining effects.
- Bulk shrinkage in non-expanding Portland cements increases strongly with increasing effective confining pressure or, equivalently, with delayed or otherwise limited access to external fluid supply. Conversely, the amount of chemical shrinkage did not vary much with effective stress state. Bulk shrinkage is observed over the entire effective confining pressure range tested.
- Comparing the different expanding cements, chemical shrinkage increases for higher MgO-CEA concentrations, because of the large negative volume change of reaction associated with MgO hydration. In absence of expansion (i.e. porosity-generating) mechanisms, this increased chemical shrinkage might enhance self-desiccation and autogenous shrinkage.
- MgO-based CEAs (5–20% bwoc) produce a significant bulk expansion effect, but this diminishes markedly under higher effective confining pressures or upon delayed external water supply. All cements tested are found unable to achieve net bulk expansion in absence of external fluid supply. However, the expanding cements show less autogenous shrinkage compared to the E0 cement, under all fluid-access conditions tested.
- The previous point may impact the volume behaviour of internal plugs, i.e. cement hydrating inside casing pipe. Note, however, that this scenario differs from the situation in the LABCAT. Bulk shrinkage of internal plugs would lead to debonding (unlike an EPDM sleeve, the casing pipe does not move inward with the cement), thus creating potential pathways for ingress of external fluids along the axial direction of the wellbore, which in turn could help limit bulk shrinkage. Since most casings can be expected to provide sufficient confinement, use of CEA concentrations higher than customary in current practice (>5% bwoc) may benefit internal cement plugs.
- At low maximum effective confining pressures (0.2–2 bar) or unrestricted external water supply, use of MgO-CEAs can cause excessive expansions (>5%), leading to microcracking. Unfortunately, separation of FoC-induced and drying-effects in the microstructural analysis proved problematic. Unlike in the LABCAT, the achievable stress-bulk strain response in many real wellbore scenarios will be limited by the stiffness of the surrounding casing pipe and rock formations. Considering bulk expansion in the LABCAT diminished rapidly with increasing effective confining pressure (<50 bar), excessive expansion downhole seems unlikely. In practice, the maximum force produced appears to be limited by the strength of the evolving cement matrix, which will generally tend to compact, rather than by the maximum FoC predicted by thermodynamics.
- While additional research is needed to investigate effects of constant strain boundary conditions, this study provides valuable insight regarding the impact of subsurface curing conditions on the volumetric behaviour of expanding cements. The findings will help define preliminary guidelines for the amounts of CEAs required to achieve cement seals with appropriate transport properties, i.e. manageable internal porosity but sufficient expansion to avoid micro-annuli, while taking the hydrodynamical and geomechanical conditions during cement curing into account.

CRediT authorship contribution statement

T.K.T. Wolterbeek: Methodology, Formal analysis, Investigation, Writing – Original draft, Visualization
E.K. Cornelissen: Methodology, Investigation
S.J.T. Hangx: Writing – Review & editing, Project administration
C.J. Spiers: Writing – Review & editing, Supervision.

Declaration of competing interest

The authors declare that they have no known competing financial interests or personal relationships that could have appeared to influence the work reported in this paper.

Acknowledgements

We would like to thank Rien Groenewegen, Thony van der Gon-Netscher, Gerard Kuijper, Floris van Oort and Leonard Bik for assistance in the laboratory. We thank an anonymous reviewer for their constructive feedback. This research was funded by Shell Global Solutions International B.V., under Amended Contract PT63253.

Appendix A. Supplementary data

Supplementary data to this article can be found online at https://doi.org/10.1016/j.cemconres.2021.106514.

References

[1] J.R. Hill, Improvement in oil-well drilling, Patent US112596A, 1871.
[2] E.B. Nelson, D. Guillot, eds., Well Cementing, second edi, Schlumberger, Sugar Land, TX 77478, USA, 2006.
[3] R.J. Davies, S. Almond, R.S. Ward, R.B. Jackson, C. Adams, F. Worrall, L. G. Herringshaw, J.G. Gluyas, M.A. Whitehead, Oil and gas wells and their integrity: implications for shale and unconventional resource exploitation, Mar. Pet. Geol. 56 (2014) 239–254.
[4] A.R. Ingraffea, M.T. Wells, R.L. Santoro, S.B.C. Shonkoff, Assessment and risk analysis of casing and cement impairment in oil and gas wells in Pennsylvania, 2000–2012, Proc. Natl. Acad. Sci. 111 (2014) 10955–10960, https://doi.org/10.1073/pnas.1323422111.
[5] S. Bachu, T. Watson, Possible indicators for CO2 leakage along wells, in: 8th Int. Conf. Greenh. Gas Control Technol., 2006: pp. 19–22.
[6] S.E. Gasda, S. Bachu, M.A. Celia, Spatial characterization of the location of potentially leaky wells penetrating a deep saline aquifer in a mature sedimentary basin, Environ. Geol. 46 (2004) 707–720, https://doi.org/10.1007/s00254-004-1073-5.
[7] T.K.T. Wolterbeek, F. Ruckert, S.G. van Moorsel, E.K. Cornelissen, Reactive transport and permeability evolution in wellbore defects exposed to periodic pulses of CO2-rich water, Int. J. Greenhouse Gas Control 91 (2019) 102835, https://doi.org/10.1016/j.ijggc.2019.102835.
[8] J.F. Heathman, F.E. Beck, Finite element analysis couples casing and cement designs for HTHP wells in East Texas, in: IADC/SPE Drill, Conf, Society of Petroleum Engineers, 2006.
[9] J. De Andrade, S. Sangesland, J. Todorovic, T. Vrålstad, Cement sheath integrity during thermal cycling: a novel approach for experimental tests of cement systems, in: SPE Bergen One Day Semin., Society of Petroleum Engineers, 2015.
[10] K.J. Goodwin, R.J. Crook, Cement sheath stress failure, SPE Drill. Eng. 7 (1992) 291–296.
[11] B. Lecampion, A. Bunger, J. Kear, D. Quesada, Interface debonding driven by fluid injection in a cased and cemented wellbore: modeling and experiments, Int. J. Greenhouse Gas Control 18 (2013) 208–223, https://doi.org/10.1016/j.ijggc.2013.07.012.
[12] B. Orlic, Some geomechanical aspects of geological CO2 sequestration, KSCE J. Civ. Eng. 13 (2009) 225–232, https://doi.org/10.1007/s12205-009-0225-2.
[13] T.K.T. Wolterbeek, S.J.T. Hangx, C.J. Spiers, Effect of CO2-induced reactions on the mechanical behaviour of fractured wellbore cement, Geomech. Energy Environ. 7 (2016) 26–46, https://doi.org/10.1016/j.gete.2016.02.002.
[14] J. Saint-Marc, A. Garnier, A.-P. Bois, Initial State of Stress: The Key to Achieving Long-term Cement-sheath Integrity, 2008, https://doi.org/10.2118/116651-MS.
[15] M. Thiercelin, B. Dargaud, J.F. Baret, W.J. Rodriquez, Cement design based on cement mechanical response, in: SPE Annu. Tech. …, 1997, pp. 266–273. https://www.onepetro.org/conference-paper/SPE-38598-MS. (Accessed 18 August 2014).
[16] I. Barclay, J. Pellenbarg, F. Tettero, J. Pfeiffer, The beginning of the end: a review of abandonment and decommissioning practices, Oilf. Rev. (2001) 28–41. http://www.slb.com/~/media/Files/resources/oilfield_review/ors01/win01/p28_41.pdf. (Accessed 18 August 2014).
[17] M.B. Dusseault, M.N. Gray, P. a Nawrocki, Why oilwells leak: cement behavior and long-term consequences, in: SPE Int. Oil Gas Conf. Exhib. SPE 64733, 2000: p. 8. doi:https://doi.org/10.2118/64733-MS.
[18] G. Daccord, D. Guillot, S. James, Remedial cementing, in: E.B. Nelson, D. Guillot (Eds.), Well Cem., Schlumberger, Sugar Land, TX 77478, USA, 2006: p. 773.
[19] J. Heathman, R. Carpenter, Quality management alliance eliminates plug failures, in: SPE Annu, Tech. Conf. Exhib, Society of Petroleum Engineers, 1994.
[20] N. Agbasimalo, M. Radonjic, Experimental study of the impact of drilling fluid contamination on the integrity of cement–formation interface, J. Energy Resour. Technol. 136 (2014) 42908, https://doi.org/10.1115/1.4027566.
[21] H.K.J. Ladva, B. Craster, T.G.J. Jones, G. Goldsmith, D. Scott, The cement-to-formation interface in zonal isolation, SPE Drill. Complet. 20 (2005). doi:https://doi.org/10.2118/88016-PA.
[22] R.C. Haut, R.J. Crook, Primary cementing: the mud displacement process, in: SPE Annu. Tech. Conf. Exhib. 23–26 Sept. Las Vegas, Nevada, Society of Petroleum Engineers, 1979. doi:https://doi.org/10.2118/8253-MS.
[23] P. Kolchanov, D. Perroni, A. Medvedev, Y. Gao, R. Tercero, L. Todd, B. Lungwitz, K.M. Cowan, W. Turner, Effective zonal isolation in horizontal wells: mitigating negative impact of mud channels, in: SPE Annu, Tech. Conf. Exhib, Society of Petroleum Engineers, 2018.
[24] G. Daccord, D. Guillot, F. Nillson, Mud removal, in: E.B. Nelson, D. Guillot (Eds.), Well Cem., 2nd ed., Schlumberger, Sugar Land, TX 77478, USA, 2006: p. 773.
[25] P. Lura, O.M. Jensen, K. Van Breugel, Autogenous shrinkage in high-performance cement paste: an evaluation of basic mechanisms, Cem. Concr. Res. 33 (2003) 223–232.
[26] P. Lura, O.M. Jensen, J. Weiss, Cracking in cement paste induced by autogenous shrinkage, Mater. Struct. 42 (2009) 1089–1099.
[27] E. Tazawa, S. Miyazawa, T. Kasai, Chemical shrinkage and autogenous shrinkage of hydrating cement paste, Cem. Concr. Res. 25 (1995) 288–292.
[28] P. Acker, Swelling, shrinkage and creep: a mechanical approach to cement hydration, Mater. Struct. 37 (2004) 237–243.
[29] H. Ye, A. Radlińska, A review and comparative study of existing shrinkage prediction models for portland and non-portland cementitious materials, Adv. Mater. Sci. Eng. 2016 (2016).
[30] H. Le Chatelier, Sur les changements de volume qui accompagnent le durcissement des ciments, Bull. Soc. l'encouragement Pour l'industrie Natl. (1900).
[31] T. Matschei, B. Lothenbach, F.P. Glasser, Thermodynamic properties of Portland cement hydrates in the system CaO–Al2O3–SiO2–CaSO4–CaCO3–H2O, Cem. Concr. Res. 37 (2007) 1379–1410.
[32] T.C. Powers, T.L. Brownyard, Studies of the physical properties of hardened Portland cement paste, 551 Bulletin 22, 1948, Research Laboratories of the Portland Cement Association, Skokie, IL, reprinted 552 from J, Am. Concr. Inst. 43 (1947) 101–132.
[33] H.J.H. Brouwers, A Hydration Model of Portland Cement Using the Work of Powers and Brownyard, 2011.
[34] M. Geiker, T. Knudsen, Chemical shrinkage of Portland cement pastes, Cem. Concr. Res. 12 (1982) 603–610.
[35] N. Agofack, S. Ghabezloo, J. Sulem, Chemo-poro-elastoplastic modelling of an oilwell cement paste: macroscopic shrinkage and stress-strain behaviour, Cem. Concr. Res. 132 (2020) 106046.
[36] M.D. Cohen, J. Olek, W.L. Dolch, Mechanism of plastic shrinkage cracking in portland cement and portland cement-silica fume paste and mortar, Cem. Concr. Res. 20 (1990) 103–119.
[37] B.R. Reddy, Y. Xu, K. Ravi, D.W. Gray, P. Pattillo, Cement shrinkage measurement in oilwell cementing-a comparative study of laboratory methods and procedures, in: Rocky Mt, Oil Gas Technol. Symp, Society of Petroleum Engineers, 2007.
[38] J. van Eijden, E. Cornelissen, F. Ruckert, T. Wolterbeek, Development of experimental equipment and procedures to evaluate zonal isolation and well abandonment materials, in: SPE/IADC Drill, Conf. Exhib, Society of Petroleum Engineers, 2017.
[39] K. Ravi, M. Bosma, O. Gastebled, Safe and Economic Gas Wells Through Cement Design for Life of the Well, SPE 75700, 2002.
[40] R. Ghofrani, H. Plack, CaO- and/or MgO-swelling cements: a key for providing a better annular sealing?, in: SPE/IADC Drill, Conf, Society of Petroleum Engineers, 1993, https://doi.org/10.2118/25697-MS.
[41] N. Jafariesfad, Y. Gong, M.R. Geiker, P. Skalle, Nano-sized mgo with engineered expansive property for oil well cement systems, in: SPE Bergen One Day Semin., Society of Petroleum Engineers, 2016.
[42] N. Jafariesfad, M.R. Geiker, Y. Gong, P. Skalle, Z. Zhang, J. He, Cement sheath modification using nanomaterials for long-term zonal isolation of oil wells, J. Pet. Sci. Eng. 156 (2017) 662–672.
[43] T. Vrålstad, A. Saasen, E. Fjær, T. Øia, J.D. Ytrehus, M. Khalifeh, Plug & abandonment of offshore wells: ensuring long-term well integrity and cost-efficiency, J. Pet. Sci. Eng. 173 (2019) 478–491.
[44] M. Oyarhossein, M.B. Dusseault, Wellbore stress changes and microannulus development because of cement shrinkage, in: 49th US Rock Mech, Symp, American Rock Mechanics Association, 2015.
[45] S.R.K. Jandhyala, G. Pangu, A. Deshpande, T. Wolterbeek, E. Cornelissen, J. van Eijden, Volume change of cement plugs: spotlight on the role of boundary conditions using an improved testing method, in: SPE Asia Pacific Oil Gas Conf, Exhib, Society of Petroleum Engineers, 2018.
[46] M.G.R. Bosma, E.K. Cornelissen, A. Schwing, Improved experimental characterisation of cement/rubber zonal isolation materials, in: Int, Oil Gas Conf. Exhib, China, Society of Petroleum Engineers, 2000.
[47] J. Zhang, E.A. Weissinger, S. Peethamparan, G.W. Scherer, Early hydration and setting of oil well cement, Cem. Concr. Res. 40 (2010) 1023–1033.
[48] N. Agofack, S. Ghabezloo, J. Sulem, A. Garnier, C. Urbanczyk, Experimental investigation of the early-age mechanical behaviour of oil-well cement paste, Cem. Concr. Res. 117 (2019) 91–102.
[49] M.E. Chenevert, B.K. Shrestha, Chemical shrinkage properties of oilfield cements (includes associated paper 23477), SPE Drill. Eng. 6 (1991) 37–43.
[50] F.L. Sabins, D.L. Sutton, Interrelationship between critical cement properties and volume changes during cement setting, SPE Drill. Eng. 6 (1991) 88–94.
[51] H. Justnes, D. Van Loo, B. Reyniers, P. Skalle, J. Sveen, E.J. Sellevold, Chemical shrinkage of oil well cement slurries, Adv. Cem. Res. 7 (1995) 85–90.
[52] C. Baumgarte, M. Thiercelin, D. Klaus, Case studies of expanding cement to prevent microannular formation, in: SPE Annu, Tech. Conf. Exhib, Society of Petroleum Engineers, 1999.
[53] V.C. Goboncan, R.L. Dillenbeck, Real-time cement expansion/shrinkage testing under downhole conditions for enhanced annular isolation, in: SPE/IADC Drill, Conf, Society of Petroleum Engineers, 2003.
[54] T. Sasaki, K. Soga, M. Abuhaikal, Water absorption and shrinkage behaviour of early-age cement in wellbore annulus, J. Pet. Sci. Eng. 169 (2018) 205–219.

[55] P.A. Parcevaux, P.H. Sault, Cement shrinkage and elasticity: a new approach for a good zonal isolation, in: SPE Annu, Tech. Conf. Exhib, Society of Petroleum Engineers, 1984.
[56] F. Rajabipour, G. Sant, J. Weiss, Interactions between shrinkage reducing admixtures (SRA) and cement paste's pore solution, Cem. Concr. Res. 38 (2008) 606–615.
[57] P. Zhan, Z. He, Application of shrinkage reducing admixture in concrete: a review, Constr. Build. Mater. 201 (2019) 676–690.
[58] I. Maruyama, K. Beppu, R. Kurihara, A. Furuta, Action mechanisms of shrinkage reducing admixture in hardened cement paste, J. Adv. Concr. Technol. 14 (2016) 311–323.
[59] V. Slowik, T. Hübner, M. Schmidt, B. Villmann, Simulation of capillary shrinkage cracking in cement-like materials, Cem. Concr. Compos. 31 (2009) 461–469.
[60] V. Baroghel-Bouny, P. Mounanga, A. Khelidj, A. Loukili, N. Rafai, Autogenous deformations of cement pastes: part II. W/C effects, micro–macro correlations, and threshold values, Cem. Concr. Res. 36 (2006) 123–136.
[61] P. Mounanga, V. Baroghel-Bouny, A. Loukili, A. Khelidj, Autogenous deformations of cement pastes: part I. Temperature effects at early age and micro–macro correlations, Cem. Concr. Res. 36 (2006) 110–122.
[62] A. Bentur, S. Igarashi, K. Kovler, Prevention of autogenous shrinkage in high-strength concrete by internal curing using wet lightweight aggregates, Cem. Concr. Res. 31 (2001) 1587–1591.
[63] P. Lura, Autogenous Deformation and Internal Curing of Concrete., (2003).
[64] J. Liu, C. Shi, X. Ma, K.H. Khayat, J. Zhang, D. Wang, An overview on the effect of internal curing on shrinkage of high performance cement-based materials, Constr. Build. Mater. 146 (2017) 702–712.
[65] D. Snoeck, L. Pel, N. De Belie, The water kinetics of superabsorbent polymers during cement hydration and internal curing visualized and studied by NMR, Sci. Rep. 7 (2017) 1–14.
[66] S. Igarashi, A. Watanabe, Experimental study on prevention of autogenous deformation by internal curing using super-absorbent polymer particles, in: Int, RILEM Publications SARL Lyngby, RILEM Conf. Vol. Chang. Hardening Concr. Test. Mitig, 2006, pp. 77–86.
[67] M.M. Al-Darbi, N.O. Saeed, L.O. Ajijolaiya, M.R. Islam, A novel oil well cementing technology using natural fibers, Pet. Sci. Technol. 24 (2006) 1267–1282.
[68] J. Zhang, V.C. Li, Influences of fibers on drying shrinkage of fiber-reinforced cementitious composite, J. Eng. Mech. 127 (2001) 37–44.
[69] S. Kawashima, S.P. Shah, Early-age autogenous and drying shrinkage behavior of cellulose fiber-reinforced cementitious materials, Cem. Concr. Compos. 33 (2011) 201–208.
[70] B. Craeye, G. De Schutter, B. Desmet, J. Vantomme, G. Heirman, L. Vandewalle, Ö. Cizer, S. Aggoun, E.H. Kadri, Effect of mineral filler type on autogenous shrinkage of self-compacting concrete, Cem. Concr. Res. 40 (2010) 908–913.
[71] L.G. Carter, H.F. Waggoner, C. George, Expanding cements for primary cementing, in: J. Pet. Technol., Soc Petroleum Eng 222 Palisades Creek Dr, Richardson, TX 75080, 1965: p. 1065.
[72] C. Wang, X. Chen, L. Wang, H. Ma, R. Wang, A novel self-generating nitrogen foamed cement: the preparation, evaluation and field application, J. Nat. Gas Sci. Eng. 44 (2017) 131–139.
[73] P.K. Weyl, Pressure solution and the force of crystallization: a phenomenological theory, J. Geophys. Res. 64 (1959) 2001–2025.
[74] G.F. Becker, A.L. Day, The linear force of growing crystals, Proc. Wash. Acad. Sci. 8 (1905) 238–288.
[75] G.T. Ostapenko, Excess Pressure on the Solid Phases Generated by Hydration (According to Experimental Data on the Hydration of Periclase), Traslated From Geokhimikiya vol. 6, 1976, pp. 824–844.
[76] X. Zheng, B. Cordonnier, W. Zhu, F. Renard, B. Jamtveit, Effects of confinement on reaction-induced fracturing during hydration of periclase, Geochem. Geophys. Geosyst. 19 (2018) 2661–2672.
[77] R.M. Skarbek, H.M. Savage, P.B. Kelemen, D. Yancopoulos, Competition between crystallization-induced expansion and creep compaction during gypsum formation, and implications for serpentinization, J. Geophys. Res. Solid Earth 123 (2018) 5372–5393.
[78] R.L.M. Vissers, T.K.T. Wolterbeek, Native copper formation in mine-prop wood from Cyprus illustrates displacive growth by force of crystallization, J. Struct. Geol. 130 (2020) 103927, https://doi.org/10.1016/j.jsg.2019.103927.
[79] S. Taber, The growth of crystals under external pressure, Am. J. Sci. (1916) 532–556.
[80] G.F. Becker, A.L. Day, Note on the linear force of growing crystals, J. Geol. 24 (1916) 313–333.
[81] M. Steiger, Crystal growth in porous materials—I: the crystallization pressure of large crystals, J. Cryst. Growth 282 (2005) 455–469, https://doi.org/10.1016/j.jcrysgro.2005.05.007.
[82] M. Steiger, Crystal growth in porous materials—II: influence of crystal size on the crystallization pressure, J. Cryst. Growth 282 (2005) 470–481, https://doi.org/10.1016/j.jcrysgro.2005.05.008.
[83] C.W. Correns, W. Steinborn, Experimente zur Messung und Erklärung der sogenannten Kristallisationskraft, Zeitschrift Für Krist. Mater. 101 (1939) 117–133.
[84] C.W. Correns, Growth and dissolution of crystals under linear pressure, Discuss. Faraday Soc. 5 (1949) 267–271.
[85] R.J. Flatt, M. Steiger, G.W. Scherer, A commented translation of the paper by C. W. Correns and W. Steinborn on crystallization pressure, Environ. Geol. 52 (2006) 187–203, https://doi.org/10.1007/s00254-006-0509-5.
[86] T.K.T. Wolterbeek, R. van Noort, C.J. Spiers, Reaction-driven casing expansion: potential for wellbore leakage mitigation, Acta Geotech. (2018) 1–26, https://doi.org/10.1007/s11440-017-0533-5.
[87] R. van Noort, T.K.T. Wolterbeek, M.R. Drury, M.T. Kandianis, C.J. Spiers, The force of crystallization and fracture propagation during in-situ carbonation of peridotite, Minerals 7 (2017), https://doi.org/10.3390/min7100190.
[88] N. Tsui, R.J. Flatt, G.W. Scherer, Crystallization damage by sodium sulfate, J. Cult. Herit. 4 (2003) 109–115, https://doi.org/10.1016/S1296-2074(03)00022-0.
[89] R.M. Espinosa Marzal, G.W. Scherer, Crystallization of sodium sulfate salts in limestone, Environ. Geol. 56 (2008) 605–621, https://doi.org/10.1007/s00254-008-1441-7.
[90] H.F.W. Taylor, Cement Chemistry, Academic Press Limited, London, UK, 1992.
[91] H.F. Taylor, C. Famy, K. Scrivener, Delayed ettringite formation, Cem. Concr. Res. 31 (2001) 683–693, https://doi.org/10.1016/S0008-8846(01)00466-5.
[92] R.J. Flatt, G.W. Scherer, Thermodynamics of crystallization stresses in DEF, Cem. Concr. Res. 38 (2008) 325–336, https://doi.org/10.1016/j.cemconres.2007.10.002.
[93] R.L. Root, D.G. Calvert, The real story of cement expansion, in: SPE Rocky Mt, Reg. Meet, Society of Petroleum Engineers, 1971.
[94] A. Klein, G.E. Troxell, Studies of Calcium Sulfoaluminate Admixures for Expansive Cements, Pros, 1958.
[95] R.M. Beirute, True expansive characteristics of commercially available expansive cement under actual well conditions, in: SPE Annu, Fall Tech. Conf. Exhib, Society of Petroleum Engineers, 1976.
[96] L. Zheng, C. Xuehua, T. Mingshu, MgO-type delayed expansive cement, Cem. Concr. Res. 21 (1991) 1049–1057.
[97] D. Appah, New Insights Into CaO-swelling Cements, 2002.
[98] L. Mo, D.K. Panesar, Effects of accelerated carbonation on the microstructure of Portland cement pastes containing reactive MgO, Cem. Concr. Res. 42 (2012) 769–777.
[99] R. Ghofrani, H. Plack, Entwicklung und Erprobung von Quellzementen für Erdgasbohrungen: DGMK-Projekt 444-2;[Forschungsbericht 444-2], Abschlußbericht, DGMK, 1994.
[100] R. Ghofrani, Development of CaO-and MgO-swelling cements into usage maturity for cementation of natural gas underground storage wells and natural gas production wells, Forschungsbericht-DGMK Dtsch, Wissenschaftliche Gesellschaft fur Erdol Erdgas und Kohle Ev, 1997.
[101] R. Ghofrani, H. Plack, Untersuchungen zur Wirksamkeit von CaO-und MgO-Quellzementen für Tiefbohrungen: DGMK-Forschungsbericht 444-1;[Forschungsbericht 444-1]; Abschlußbericht zur Vorphase des DGMK-Projektes 444, Entwicklung und Erprobung von Quellzementen für Erdgasbohrungen, DGMK, 1993.
[102] S. Chatterji, Mechanism of expansion of concrete due to the presence of dead-burnt CaO and MgO, Cem. Concr. Res. 25 (1995) 51–56.
[103] L. Mo, M. Deng, M. Tang, A. Al-Tabbaa, MgO expansive cement and concrete in China: past, present and future, Cem. Concr. Res. 57 (2014) 1–12.
[104] L. Zheng, C. Xuehua, T. Mingshu, Hydration and setting time of MgO-type expansive cement, Cem. Concr. Res. 22 (1992) 1–5.
[105] B. Lothenbach, T. Matschei, G. Möschner, F.P. Glasser, Thermodynamic modelling of the effect of temperature on the hydration and porosity of Portland cement, Cem. Concr. Res. 38 (2008) 1–18.
[106] D.L. Bour, D. Daugherty, D.L. Sutton, New expansive cement system for high temperature, Proc. 1988 Southwest. Pet. Shourt Course. Southwest. Pet. (1988) 1–9.
[107] D.R. Glasson, Reactivity of lime and related oxides. II. Sorption of water vapour on calcium oxide, J. Appl. Chem. 8 (1958) 798–803.
[108] F. Jin, A. Al-Tabbaa, Characterisation of different commercial reactive magnesia, Adv. Cem. Res. 26 (2014) 101–113, https://doi.org/10.1680/adcr.13.00004.
[109] X. Tang, L. Guo, C. Chen, Q. Liu, T. Li, Y. Zhu, The analysis of magnesium oxide hydration in three-phase reaction system, J. Solid State Chem. 213 (2014) 32–37, https://doi.org/10.1016/j.jssc.2014.01.036.
[110] R. Salomão, C.C. Arruda, A.D. V Souza, L. Fernandes, Novel insights into MgO hydroxylation: effects of testing temperature, samples' volume and solid load, Ceram. Int. 40 (2014) 14809–14815. doi:doi:https://doi.org/10.1016/j.ceramint.2014.06.074.
[111] V. Kasselouris, C. Ftikos, G. Parissakis, On the hydration of MgO in cement pastes hydrated up to eight years, Cem. Concr. Res. 15 (1985) 758–764.
[112] H.S. Meissner, Cracking in concrete due to expansive reaction between aggregate and high-alkali cement as evidenced in Parker Dam, in: J. Proc., 1941: pp. 549–568.
[113] P.K. Mehta, History and status of performance tests for evaluation of soundness of cements, in: Cem, Stand, Trends, ASTM International, 1978.
[114] I. Odler, Free lime content and unsoundness of cement, Mater. Sci. Concr. Spec. (2001) 237–244.
[115] A. Nawaz, P. Julnipitawong, P. Krammart, S. Tangtermsirikul, Effect and limitation of free lime content in cement-fly ash mixtures, Constr. Build. Mater. 102 (2016) 515–530.
[116] F.C. Caner, Z.P. Bažant, Lateral confinement needed to suppress softening of concrete in compression, J. Eng. Mech. 128 (2002) 1304–1313.
[117] Y. Li, Y. Lu, R. Ahmed, B. Han, Y. Jin, Nonlinear stress-strain model for confined well cement, Materials (Basel). 12 (2019) 2626.
[118] Z.P. Bazant, F.C. Bishop, T.-P. Chang, Confined compression tests of cement paste and concrete up to 300 ksi, ACI J. 33 (1986) 553–560.

[119] Z.P. Bazant, J.J.H. Kim, M. Brocca, Finite strain tube-squash test of concrete at high pressures and shear angles up to 70 degrees, ACI Mater. J. 96 (1999) 580–592.
[120] ISO 10426-5, Petroleum and natural gas industries - cements and materials for well cementing - part 5: determination of shrinkage and expansion of well cement formulations at atmospheric pressure (API Technical Report 10TR 2), (2004).
[121] ISO 10426-2, Petroleum and natural gas industries - cements and materials for well cementing - part 2: testing of well cements (ANSI/API Recommended Practice 10B-2), (2005).
[122] API Technical Report 10TR2, Shrinkage and Expansion in Oilwell Cement, 1997.
[123] K.R. Backe, P. Skalle, O.B. Lile, S.K. Lyomov, H. Justnes, J. Sveen, Shrinkage of oil well cement slurries, J. Can. Pet. Technol. 37 (1998).
[124] N.H. Mondol, K. Bjørlykke, J. Jahren, K. Høeg, Experimental mechanical compaction of clay mineral aggregates—changes in physical properties of mudstones during burial, Mar. Pet. Geol. 24 (2007) 289–311.
[125] J. Zhang, Effective stress, porosity, velocity and abnormal pore pressure prediction accounting for compaction disequilibrium and unloading, Mar. Pet. Geol. 45 (2013) 2–11.
[126] S. Shima, M. Oyane, Plasticity theory for porous metals, Int. J. Mech. Sci. 18 (1976) 285–291.
[127] R. Narayanasamy, T. Ramesh, K.S. Pandey, Some aspects on cold forging of aluminium–iron powder metallurgy composite under triaxial stress state condition, Mater. Des. 29 (2008) 891–903.
[128] S. Asadov, M.H. Ozyurtkan, Modelling the effect additives on exothermic heat development of well cement, in: 51st US Rock Mech, Symp, American Rock Mechanics Association, 2017.